



RESEARCH PAPER



Design, synthesis, and anti-cancer evaluation of new pyrido[2,3-d]pyrimidin-4(3H)-one derivatives as potential EGFR^{WT} and EGFR^{T790M} inhibitors and apoptosis inducers

Heba S. A. Elzahabi^a , Eman S. Nossier^a, Rania A. Alasfoury^a, May El-Manawaty^b, Sara M. Sayed^c,
Eslam B. Elkaeed^d, Ahmed M. Metwaly^{e,f}, Mohamed Hagra^g and Ibrahim H. Eissa^h 

^aPharmaceutical Medicinal Chemistry & Drug Design Department, Faculty of Pharmacy (Girls), Al-Azhar University, Cairo, Egypt; ^bPharmacognosy Department, National Research Centre, Dokki, Cairo, Egypt; ^cBiochemistry and Molecular Biology Department, Faculty of Pharmacy (Girls), Al-Azhar University, Cairo, Egypt; ^dDepartment of Pharmaceutical Sciences, College of Pharmacy, AlMaarefa University, Riyadh, Saudi Arabia; ^ePharmacognosy and Medicinal Plants Department, Faculty of Pharmacy (Boys), Al-Azhar University, Cairo, Egypt; ^fBiopharmaceutical Products Research Department, Genetic Engineering and Biotechnology Research Institute, City of Scientific Research and Technological Applications (SRTA-City), Alexandria, Egypt; ^gPharmaceutical Organic Chemistry, Faculty of Pharmacy (Boys), Al-Azhar University, Cairo, Egypt; ^hPharmaceutical Medicinal Chemistry & Drug Design Department, Faculty of Pharmacy (Boys), Al-Azhar University, Cairo, Egypt

ABSTRACT

A new series of pyrido[2,3-d]pyrimidin-4(3H)-one derivatives having the essential pharmacophoric features of EGFR inhibitors has been designed and synthesised. Cell viability screening was performed for these compounds against A-549, PC-3, HCT-116, and MCF-7 cell lines at a dose of 100 μ M. The highest active derivatives (**8a**, **8b**, **8d**, **9a**, and **12b**) were selected for IC₅₀ screening. Compounds **8a**, **8b**, and **9a** showed the highest cytotoxic activities and were further investigated for wild EGFR^{WT} and mutant EGFR^{T790M} inhibitory activities. Compound **8a** showed the highest inhibitory activities against EGFR^{WT} and EGFR^{T790M} with IC₅₀ values of 0.099 and 0.123 μ M, respectively. In addition, it arrested the cell cycle at pre-G1 phase and induced a significant apoptotic effect in PC-3 cells. Furthermore, compound **8a** induced a 5.3-fold increase in the level of caspase-3 in PC-3 cells. Finally, docking studies were carried out to examine the binding mode of the synthesised compounds against both EGFR^{WT} and EGFR^{T790M}.

ARTICLE HISTORY

Received 12 January 2022
Accepted 1 April 2022

KEYWORDS

Anti-proliferative; apoptosis; docking studies; EGFR inhibitors; pyrido[2,3-d]pyrimidin-4(3H)-one

1. Introduction

According to WHO, cancer was the direct cause of 10 million deaths in 2020 and the cost of cancer treatment globally was US\$1.16 trillion in 2010¹. Several internal and external factors can cause cancer. The most well-known factors are hormonal disorders, genetic mutations, radiations, smoking tobacco, metals, polluted food, chemicals, and infectious organisms^{2–4}. Resistance against anticancer drugs is considered one of the most serious problems in cancer management⁵. Due to the high residence of many cancer types, the discovery of new anticancer agents with high effect, less resistance, and fewer side effects is an urgent need.


Protein kinases (PKs) are a group of enzymes that are responsible for the transference of phosphate from ATP molecule to tyrosine, serine and/or threonine amino acids in protein substrates^{6,7}. Furthermore, PKs promote cellular signalling processes such as cell growth regulation, differentiation, migration, and metabolism⁸. PKs have been found to be overexpressed in a variety of human malignancies⁹. Accordingly, the inhibition of PKs has emerged as a selective method for killing cancer cells¹⁰. Receptor tyrosine

kinases (RTKs) are vital category protein kinases. About 20 different RTKs have been discovered that have similar structures¹¹.

The epidermal growth factor receptor (EGFR) belongs to the RTKs family that stimulates differentiation and proliferation of cells after the binding of its specific active ligand¹². EGFR structure has an extracellular part (at the surface of the cells) and an intracellular part. The activation of the outer part leads to an activation of the intracellular region of the receptor and a phosphorylation of the intracellular substrates¹³. This step facilitates cell growth, synthesis of DNA, and the expression of oncogenes¹⁴. It was reported that EGFR is over-expressed and implicated in the pathogenesis and progression of various human carcinomas¹⁵. In many patients, resistance against cancer therapy arises from an acquired mutation in the EGFR kinase domain (T790M). Such mutant EGFR is called EGFR^{T790M16}. Thus, EGFRs (wild and mutant types) are interesting biological targets for the discovery of new anticancer agents^{17,18}.

The ATP binding site of EGFR consists of five regions; an adenine-binding pocket, a sugar region (ribose binding pocket), a hydrophobic region I, a hydrophobic region II, and a phosphate-binding region^{19–21}. Most of the reported EGFR inhibitors are ATP-competitive inhibitor small molecules that have specific moieties

CONTACT Ibrahim H. Eissa  ibrahimeissa@azhar.edu.eg  Pharmaceutical Medicinal Chemistry & Drug Design Department, Faculty of Pharmacy (Boys), Al-Azhar University, Cairo 11884, Egypt; Heba S. A. Elzahabi  hebaelzahaby@azhar.edu.eg  Pharmaceutical Medicinal Chemistry & Drug Design Department, Faculty of Pharmacy (Girls), Al-Azhar University, Cairo, Egypt

 Supplemental data for this article is available online at [here](https://doi.org/10.1080/14756366.2022.2062752).

© 2022 The Author(s). Published by Informa UK Limited, trading as Taylor & Francis Group.

This is an Open Access article distributed under the terms of the Creative Commons Attribution License (<http://creativecommons.org/licenses/by/4.0/>), which permits unrestricted use, distribution, and reproduction in any medium, provided the original work is properly cited.

to occupy the adenine-binding pocket, the hydrophobic region I, and the hydrophobic region II¹⁰ (Figure 1).

EGFR inhibitors have a specific Y-shaped structure²³. In addition, the structure of EGFR inhibitors should comprise many essential pharmacophoric features²⁴. Each feature binds at a specific region in the ATP binding site. For example, a flat hetero aromatic system is an essential feature of EGFR inhibitor to occupy the adenine binding pocket of the ATP binding site. Such hetero structure can form hydrogen bonds with some amino acids as Met769, Thr790, and Thr854²⁵. Also, a terminal hydrophobic head of the EGFR inhibitor can occupy the hydrophobic region I

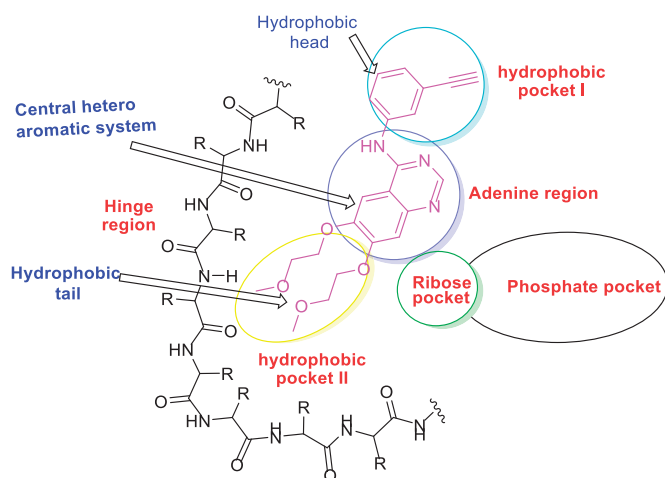


Figure 1. The essential pharmacophoric features of erlotinib as an EGFR inhibitor occupying three pockets in the ATP binding site based on Reference²².

forming many hydrophobic interactions²⁴. Finally, a hydrophobic tail be buried in the hydrophobic region II producing high affinity^{19,26}.

Till now, three generations of EGFR inhibitors were approved by the FDA (Figure 2). Erlotinib I²⁷ and gefitinib II²⁸ are examples of the first generation. The generated mutation in EGFR led to the acquired drug resistance and reduced efficacy in cancer treatment²⁹. The mutant form of protein (EGFR^{T790M}) resists the affinity of ATP-competitive inhibitors³⁰. The second-generation of EGFR inhibitors was approved to overcome the drug resistance that was induced by EGFR^{T790M}. These inhibitors can form covalent interactions with Cys797 at the ATP binding site^{31–33}. Pelitinib III³⁴ is a well-known example of this class. Unfortunately, low maximal-tolerated-dose, the major drawback of this class, led to poor clinical outcomes^{35,36}. Osimertinib 5³⁷, an example of the third-generation EGFR inhibitors, exhibited greater activities against mutant form (EGFR^{T790M}) than the wild form (EGFR^{WT}). Recently, toxic epidermal necrolysis was reported upon the administration of olmutinib³⁸. Hence, many efforts are still required to reach more potent and less toxic EGFR inhibitors.

Pyrido[2,3-d]pyrimidin-4(3H)-one moiety was utilised before for the synthesis of various anticancer agents^{39–42}, and EGFR inhibitors⁴³. Interestingly it was included in the discovery of highly specific inhibitors against the mutant EGFR^{T790M44}.

As an extension of our previous efforts in the design and synthesis of new anticancer agents^{45–51}, especially that target RTKs^{52,53} and EGFR^{22 54–58}, we used the pyrido[2,3-d]pyrimidin-4(3H)-one moiety as a building block for the design and synthesis of new anticancer agents targeting the wild EGFR (EGFR^{WT}) as well as the mutant EGFR (EGFR^{T790M}).

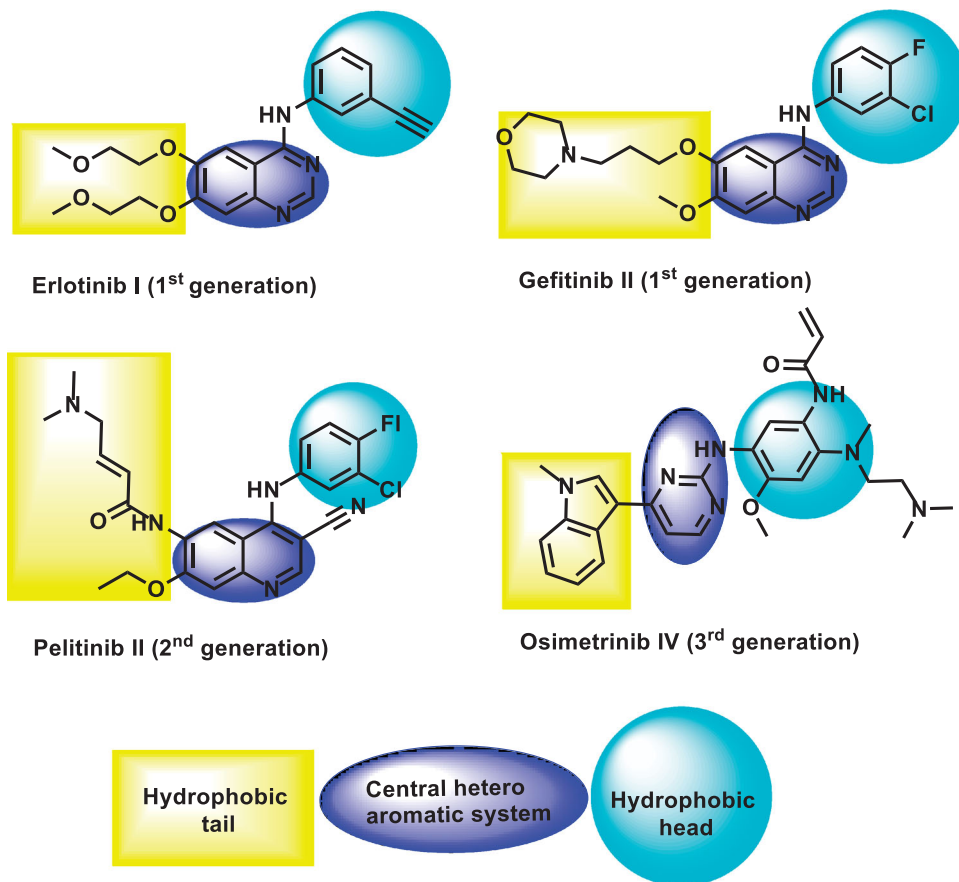


Figure 2. Some reported EGFR-TK inhibitors and their basic pharmacophoric features.

1.1. Rationale of molecular design

For years, our team synthesised several EGFR inhibitors which showed promising anticancer activities. In 2018, a series of 1H-pyrazolo[3,4-d]pyrimidine derivatives were synthesised and evaluated for their inhibitory activities against EGFR^{WT} and EGFR^{T790M}. Compound V potently inhibited the two EGFR types with a good apoptotic effect and arrested the cell cycle at the G₂/M phase. Such compounds comprise two hetero-aromatic rings (1H-pyrazolo[3,4-d]pyrimidine) to occupy the adenine binding pocket²².

In 2019, we designed and synthesised a series of thieno[2,3-d]pyrimidine derivatives as EGFR and HER2 tyrosine kinase inhibitors. Compound VI was the most active member producing significant apoptosis. This compound contains two hetero-aromatic rings (thieno[3,2-d]pyrimidine) to occupy the adenine binding pocket⁵⁴.

In 2020, our team designed and synthesised a new series of pyrimidine-5-carbonitrile derivatives as EGFR inhibitors. Compound VII showed high inhibitory activities against EGFR^{WT} and EGFR^{T790M}. In addition, it arrested the cell cycle at the G₂/M phase and induced a significant apoptotic effect in HCT-116, HepG-2, MCF-7 cells. This compound contains one hetero-aromatic ring (pyrimidine) to occupy the adenine binding pocket⁵⁵.

In the current work, we used the previously reported active candidates (V, VI, and VII)^{22,54,55} as lead compounds in the design of the new derivatives. The rationale of our molecular design depended on the modification of such compounds to get new EGFR inhibitors. The modification was carried out at three features following the essential features of EGFR inhibitors. Concerning the terminal hydrophobic head and the hydrophobic tail, different substituted benzene rings were used to study the SAR of the synthesised compounds. Regarding the flat hetero-aromatic system, we used three different systems. The first one is pyrido[2,3-d]pyrimidin-4(3H)-one moiety which comprises two hetero-aromatic rings (compounds **9a–e**). The second one is pyrido[2,3-d][1,2,4]triazolo[4,3-a]pyrimidin-5(1H)-one moiety which composes three hetero-aromatic rings (compounds **10a–d**, **11a–e**, and **12a–d**). The third one is 5H-pyrido[2',3':4,5]pyrimido[2,1-b]quinazoline-5,7(12H)-dione moiety which constitutes four hetero-aromatic rings (compounds **8a–d**; Figure 3).

2. Results and discussion

2.1. Chemistry

In continuation of the previous work⁵⁹, the starting precursor 2-thioxo-2,3-dihydropyrido[2,3-d]pyrimidin-4(1H)-one derivatives **7a–e** were afforded via the reaction of the appropriate chalcones **6a–e** with 6-aminothiouracil **3**. The target compounds were synthesised in acceptable yield as reported⁵⁹. Here in, the structure of the new 2-thioxo-2,3-dihydropyrido[2,3-d]pyrimidin-4(1H)-one derivative **7a** was proved by elemental and spectral analyses. ¹H NMR spectrum showed two D₂O exchangeable singlet signals at δ 12.51, 13.23 ppm correspond to the two protons of each NH groups. Also, a singlet signal was recorded at δ 7.97 ppm, corresponding to the proton at C6 of pyridopyrimidine ring. The ¹³C NMR spectrum of **7a** analogue displayed two characteristic signals at δ 162.29, 175.61 corresponding to carbons of C=O and C=S groups, respectively.

The 5H-pyrido[2',3':4,5]pyrimido[2,1-b]quinazoline-5,7(12H)-dione analogues **8a–d** were synthesised through the reaction of compounds **7b–e** with anthranilic acid in the presence of catalytic amount of sodium ethoxide under reflux condition⁶⁰. Their chemical structures were confirmed by elemental and spectral data for

example the ¹H NMR of compound **8d** revealed an increase in the integration of aromatic region at δ 6.76–8.15 ppm, and the presence of D₂O exchangeable singlet signal assigned for one proton of NH group at δ 11.64 ppm. The ¹³C NMR spectrum showed the characteristic two signals for the two carbons of C=O signals at δ 161.45 and 169.46 ppm. The mass spectrum for **8d** revealed the expected molecular ion peak at m/z of 520. Finally, IR spectrum of **8b** displayed absorption bands at 1693, 1750 and 3410 cm⁻¹ corresponding to two C=O and one NH groups, respectively.

The 2-hydrazinopyrido[2,3-d]pyrimidin-4(3H)-one derivatives **9a–e** were depicted through the nucleophilic attack of hydrazine hydrate upon the key derivatives **7a–e** following the reported method⁶⁰. The newly hydrazinyl derivative **9a** was proved by spectral data. The ¹H NMR spectrum showed two singlet signals at δ 8.23, 9.12 ppm assigned for three protons of hydrazinyl group NHHN₂.

Cyclo-condensation of the 2-hydrazinyl derivative **9a–e** with ethyl chloroformate in dry pyridine produced pyrido[2,3-d][1,2,4]triazolo[4,3-a]pyrimidine-3,5-dione derivatives **10a–d**. The IR spectrum of compound **10d** revealed the presence of three absorption bands at 1708, 3437, and 3425 cm⁻¹ assigned for two carbonyl and two NH groups, respectively. The ¹H NMR spectrum for the same compound showed two D₂O exchangeable signals at δ 9.26, 11.07 ppm assigned for two NH groups. Mass spectrum of compound **10c** showed molecular ion peak at m/z of 479 and its isotope at m/z of 481.

Reaction of hydrazinyl derivatives **9a–e** with ammonium thiocyanate in glacial acetic acid under reflux afforded 3-aminopyrido[2,3-d][1,2,4]triazolo[4,3-a]pyrimidin-5(1H)-one derivatives **11a–e**. The ¹H NMR of compound **11a** revealed the presence of two exchangeable singlet signals at 7.09 and 7.33 ppm assigned for NH and NH₂ groups. Mass spectra of compound **11c** illustrated the expected molecular ion peak at m/z of 400.5.

The 3-phenylpyrido[2,3-d][1,2,4]triazolo[4,3-a]pyrimidin-5(1H)-one analogues **12a–e** were obtained via the reaction of hydrazinyl derivatives **9a–e** with benzoyl chloride in pyridine under reflux conditions. Analytical and spectroscopic measurements confirmed the structures of compounds **12a–d**. The IR spectrum of **12b** displayed two absorption bands at 1720, 3414 cm⁻¹ corresponds to C=O and NH groups, respectively. The ¹H NMR spectrum of the same series gave an increase in aromatic integration due to the presence of an extra phenyl ring. The mass spectrum of **12b** revealed a molecular ion peak at m/z of 459 (Schemes 1 and 2).

2.2. Biological evaluation

2.2.1. In vitro antiproliferative activities

All the final synthesised (19) compounds were tested for their anticancer activities against four tumour cell lines namely, lung cancer (A-549), prostate cancer (PC-3), colon cancer (HCT-116), and breast cancer (MCF-7) using standard MTT method^{61–63}. Preliminary screening against the cancer cell lines was performed, using doxorubicin as a reference drug at doses of 100 μ M. Variable results were recorded for the screened compounds as depicted in Table 1. The pyrido[2,3-d]pyrimidin-4(3H)-one derivatives (**8a**, **8b**, **8d**, and **9a**) that exhibited inhibitory activity $\geq 70\%$ were selected for IC₅₀ screening comparing erlotinib.

All compounds were barely active against breast cancer (MCF-7) cell line at 100 μ M (% of inhibition ranging from 5 to 68% (Table 1). By focussing on the prostatic cell line (PC-3), the anticancer profile of the tested compounds was significantly improved especially the tetracyclic derivatives **8a** (IC₅₀ = 7.98 μ M) and **8d** (IC₅₀ = 7.12 μ M) that exhibited about 1.5 times more active than

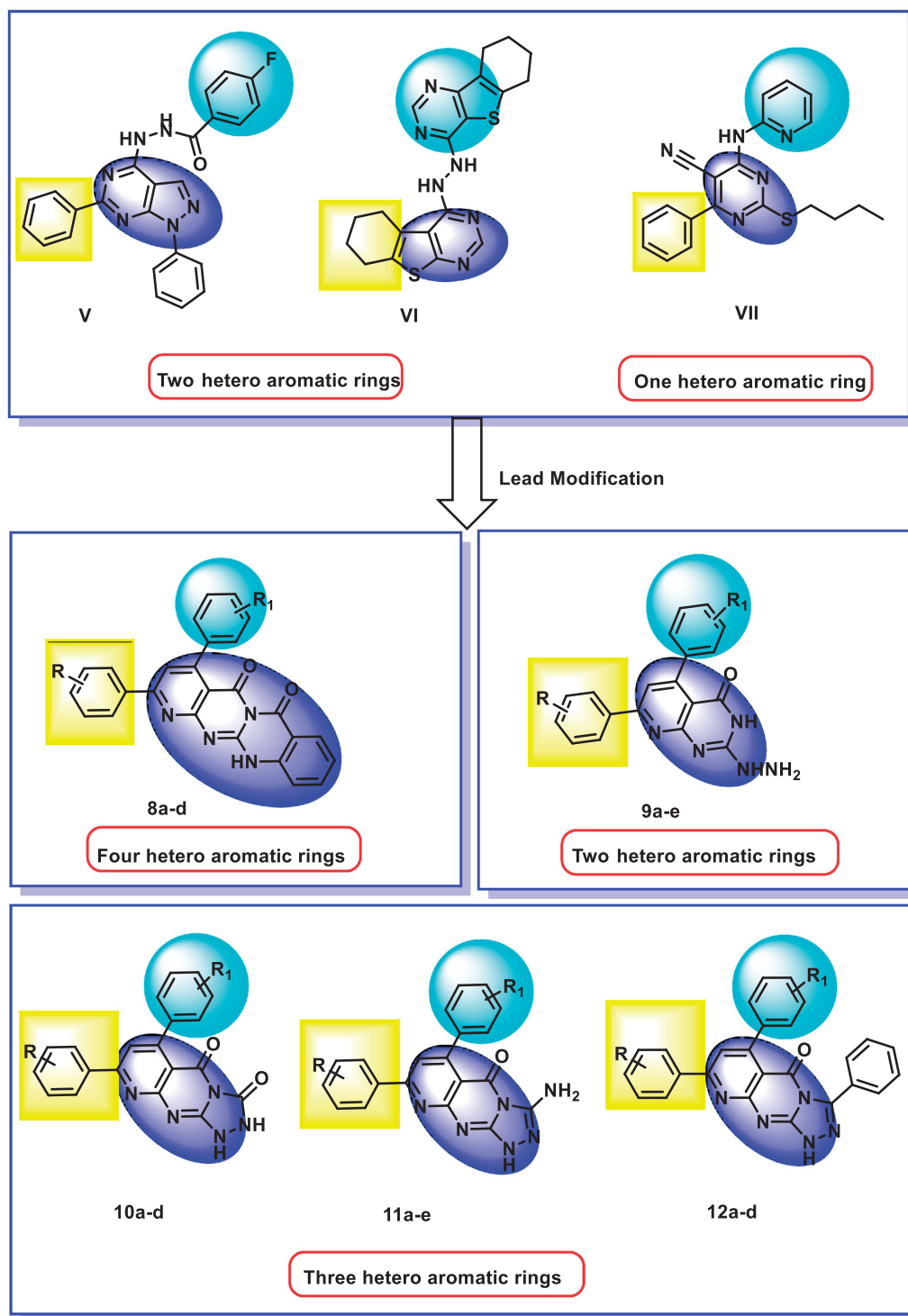


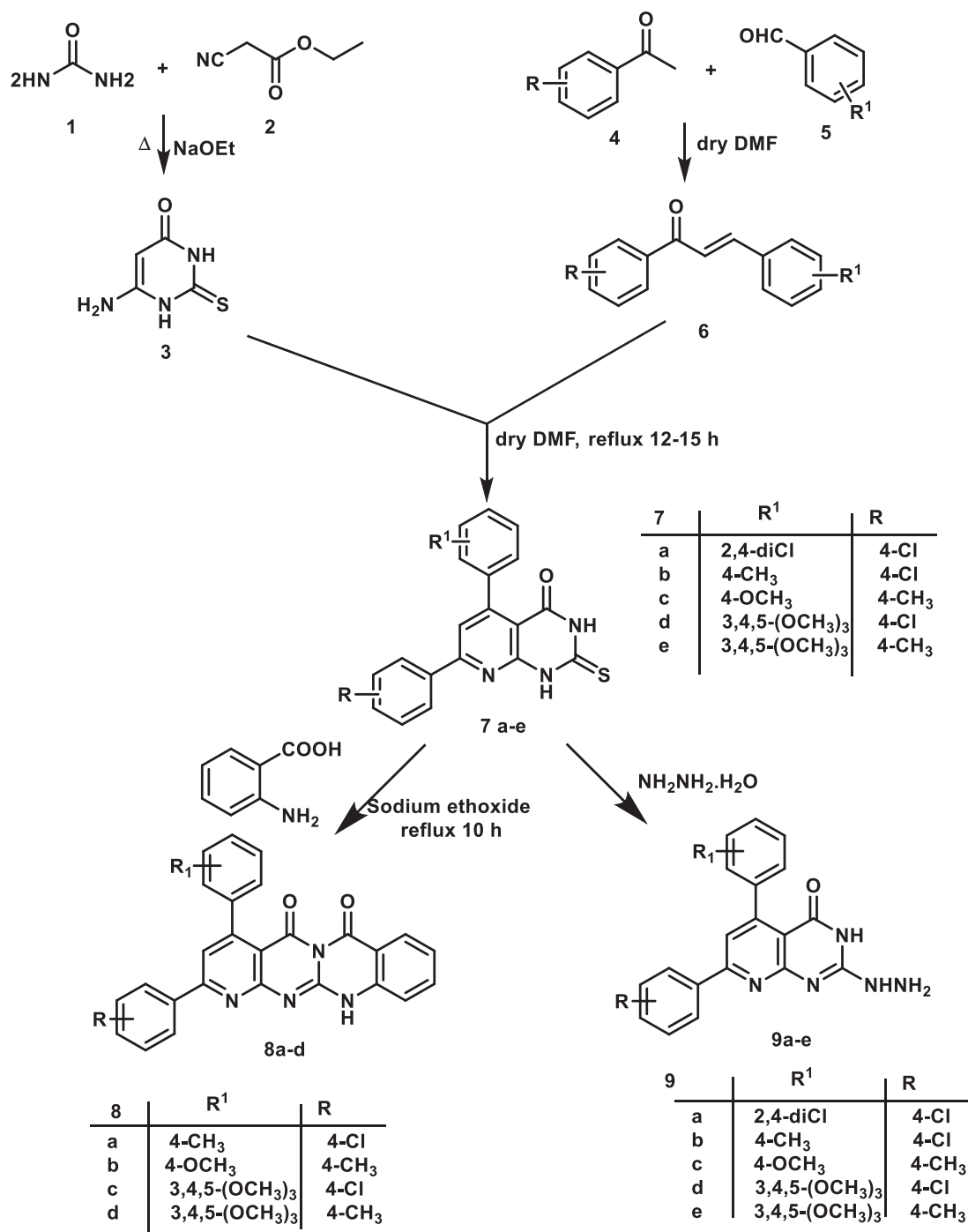
Figure 3. Synthesis of new EGFR inhibitors strategy.

erlotinib (11.05 μM). In addition, compound **9a** showed a strong activity against PC-3 line with an IC_{50} value of 9.26 μM . For compound **8d**, it showed a strong anti-proliferative activity against A-549 with an IC_{50} value of 7.23 μM which is comparable to erlotinib ($\text{IC}_{50} = 6.53 \mu\text{M}$). Compound **8b** revealed a moderate inhibitory activity against PC-3 cell line with an IC_{50} value of 18.01 μM . Generally, no cytotoxic activity was observed against the colon cancer cell line (HCT-116), but compounds **8a**, **8b**, **8d**, **12b** revealed mild cytotoxic activity.

2.2.2. Structural-activity relationship

The synthetic pathway of the target compounds was depicted in two schemes starting with thioxo-precursors **7a-e** to afford tetracyclic derivatives **8a-d**, hydrazinyl derivatives **9a-e**, and triazolyl derivatives **10a-d**, **11a-e**, and **12a-d** (Figure 4).

Expansion of pyrido[2,3-d]pyrimidin-4(3H)-one core to give tetracyclic 5H-pyrido [2',3':4,5]pyrimido[2,1-b]quinazoline-5,7(12H)-dione derivatives **8a-d** showed the preferred impact on the evaluated anticancer activity. Compounds **8a**, **b**, **d** exhibited the most



Scheme 1. General procedure for the synthesis of the target compound 7a–e, 8a–d, and 9a–e.

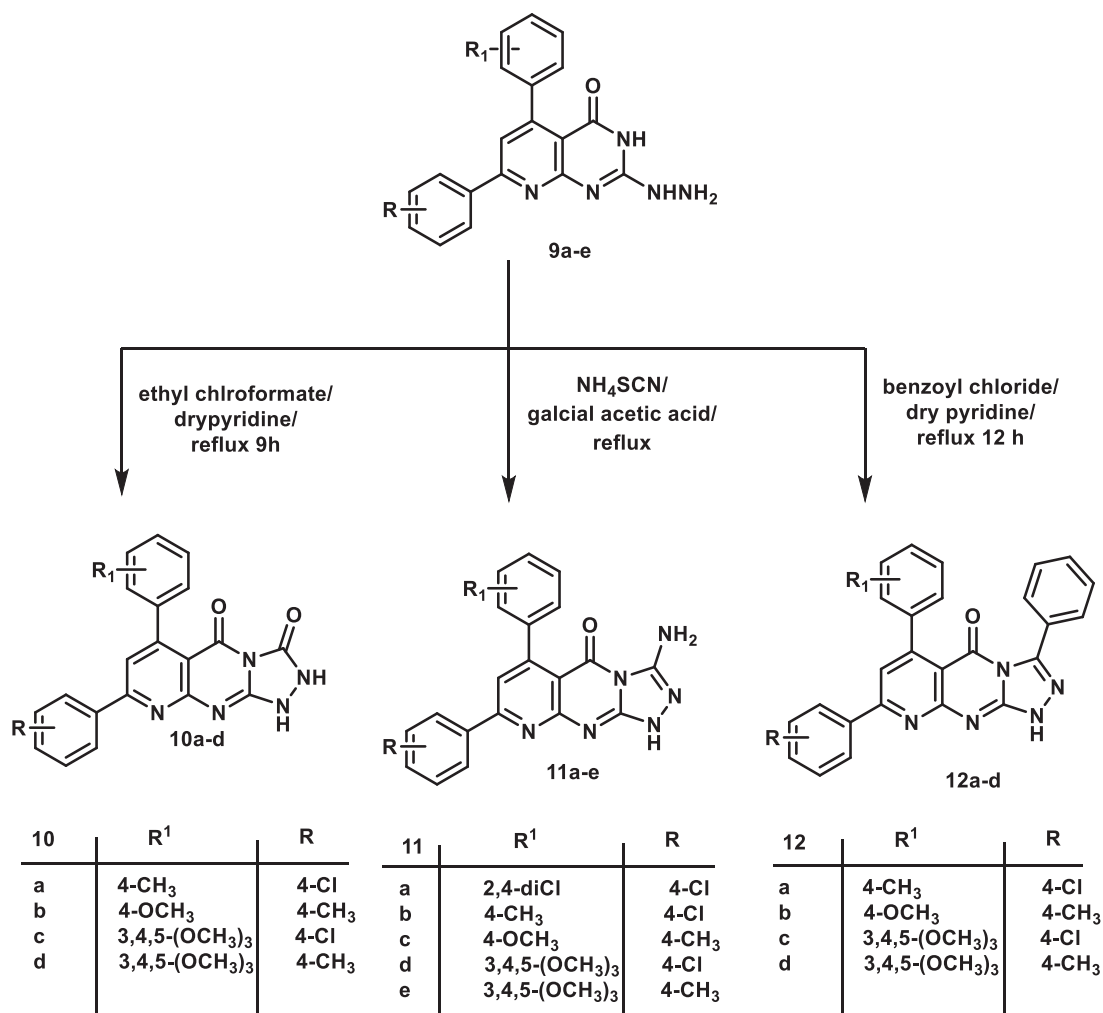
potent cytotoxic activity against A-549 cell line with IC_{50} values of 16.2, 16, and 7.23 μM , respectively, and the later was equipotent to erlotinib ($\text{IC}_{50} = 6.53 \mu\text{M}$).

Concerning prostate cancer cell line (PC-3), both compounds **8a** ($\text{IC}_{50} = 7.98 \mu\text{M}$), and **8d** ($\text{IC}_{50} = 7.12 \mu\text{M}$), were two-fold more potent than the reference molecule ($\text{IC}_{50} = 11.05 \mu\text{M}$). It was noticed that the electronic factor greatly influences the anticancer activity of the same series against lung and prostate cancer cells. For example, the existence of electron-donating (OCH_3) group at 4-position of compounds **8a** and **8d** was beneficial for activity. The modification of tetracyclic derivatives **8a** ($\text{IC}_{50} = 7.98 \mu\text{M}$) into hydrazinyl derivatives **9a** ($\text{IC}_{50} = 9.26 \mu\text{M}$) decreased the

anticancer activity against prostate cancer cell line ($\text{IC}_{50} = 9.26 \mu\text{M}$). In addition, the expansion of pyrido[2,3-d]pyrimidin-4(3H)-one scaffold into triazolyl analogues caused a remarkable drop in the activity with an inhibition range from 2 to 52% (Table 2).

2.2.3. EGFR^{WT} kinase inhibitory assay

The promising antiproliferative compounds (**8a**, **8d**, and **9a**) were further examined for their EGFR^{WT} kinase inhibitory activities using Homogeneous time resolved fluorescence (HTRF) assay⁶⁴. Erlotinib was used as a reference molecule (Table 3).



Scheme 2. General procedure for the synthesis of the target compound 10a–d, 11a–e and 12a–d.

The tested derivatives **8a**, **8d**, and **9a** showed promising inhibitory activities against EGFR^{WT} with IC₅₀ values of 0.099, 0.419, and 0.594 μM, respectively. compounds **8a** showed a good activity compared to erlotinib (IC₅₀ = 0.043 μM). Whereas compounds **8d** and **9a** showed moderate act nlp0m kinase inhibitory assay

To evaluate the potential activity of the synthesised compounds against the mutant form of EGFR, the most active cytotoxic compounds (**8a**, **8d** and **9a**) were tested for their inhibitory effect against EGFR^{T790M}. Erlotinib was used as a positive control.

The tested compounds **8a**, **8d** and **9a** showed inhibitory effects against EGFR^{T790M} with IC₅₀ values of 0.123, 0.290, and 0.571 μM, respectively. Compound **8a** exhibited the highest inhibitory effect but less than erlotinib (IC₅₀ = 0.071 μM). While compounds **8d** and **9a** showed moderate inhibitory activities (Table 3).

2.2.4. Cell cycle analysis

Based on the above-mentioned biological testing, the most promising candidate **8a** was subjected to flow cytometry analysis to investigate its effect on the cell cycle distribution in the most sensitive cell line (PC-3). The reported protocol described by Wand et al.⁶⁵ was applied in this test. PC-3 cells were incubated with compound **8a** for 24 h in a concentration equal to its IC₅₀ against

such cell line (7.98 μM). After that, the different phases of the cell cycle were analysed.

Compound **8a** showed different effects on the cell cycle distribution. Compared to the control cells (Cont. (PC-3)), the cell population increased at the phases of pre-G₁ and %S by 22 and 1.3 folds, respectively. For the Pre-G₁ phase, the cell increased from 1.78% (in cont. cells) to 41.06% (at the treated cells). In the S phase, the cell increased from 41.03% (in cont. cells) to 53.69% (at the treated cells). On the other hand, the cell population decreased in both the G₀–G₁ and the G₂–M phases. Such results obviously reveal that compound **8a** can arrest the PC-3 cell line at pre-G₁ of the cell cycle (Figure 5 and Supplementary data).

2.2.5. Annexin V-FITC apoptosis assay

To analyse the apoptotic effect of the most active compound **8a**, Annexin V and PI double staining assay with FITC was applied⁶⁶. In this test, PC-3 cells were incubated with compound **8a** at a concentration of 7.98 μM for 24 h. The results were depicted in (Figure 6 and Supplementary data).

Investigating the results of Annexin V and PI double staining assay, revealed that compound **8a** produced a significant increase in the early apoptosis ratio from 0.43 to 13.92% (32-fold). Also, it exerted an increase in the late apoptosis ratio from 0.15 to

Table 1. Percentage of growth inhibition activity of compounds **7a**, **8a-d**, **9a**, **10a-e** against A549, PC-3, HCT-116 and MCF-7 at a concentration of 100 μ M.

Comp.	Growth inhibition (%)			
	A549	PC-3	HCT-116	MCF-7
7_a	14	12	18	34
8_a	90	98	84	32
8_b	94	96	67	9
8_c	8	17	9	21
8_d	97	95	78	15
9_a	42	90	89	68
10_a	17	29	21	41
10_b	7	15	14	4
10_c	9	52	23	8
10_d	2	8	5	5
11_a	2	30	9	7
11_b	28	43	15	29
11_c	26	28	3	23
11_d	5	20	3	37
11_e	30	22	6	23
12_a	41	28	35	45
12_b	33	36	56	54
12_c	22	30	33	55
12_d	4	14	5	15
Doxorubicin	100	100	100	100

22.49% (150-fold). Such findings indicate that compound **8a** has a significant apoptotic effect against PC-3 cells.

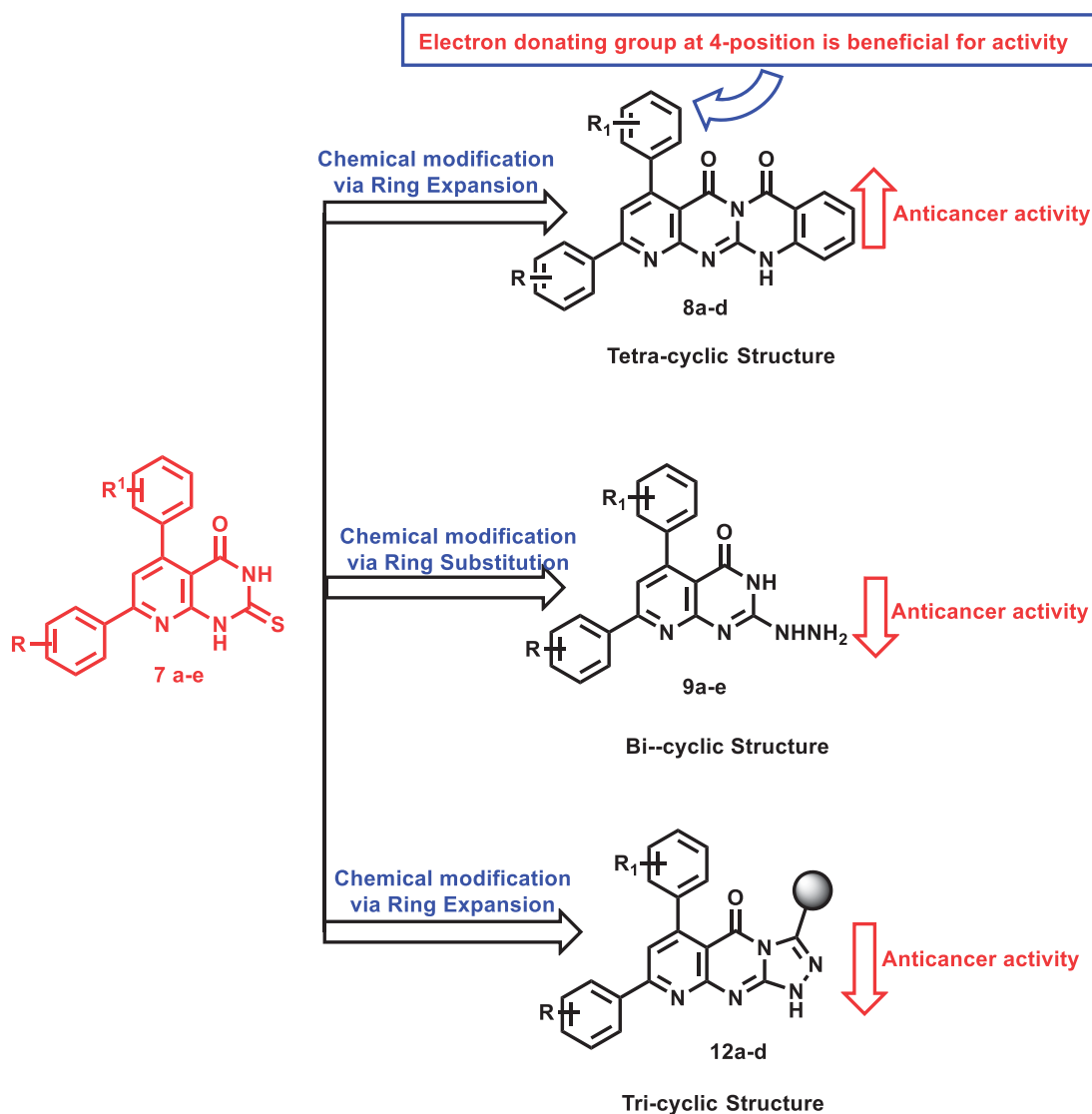
2.2.6. Caspase-3 determination

The ability of a drug to induce apoptosis determines the sensitivity of the cancer cells against it. There are many signalling pathways that control apoptosis induction. Caspases family are considered as one of the most apoptotic regulators⁶⁷. Activation of caspases especially (caspase-3) produces cell death⁶⁸. In addition, it was reported that EGFR inhibitors exhibit significant

Table 2. IC₅₀ values of compounds **8_a**, **8_b**, **8_d**, **9_a** and **12_b** against A-549, PC-3, HCT-116 and MCF-7.

Compounds	IC ₅₀ (μ M) ^a			
	A-549	PC-3	HCT-116	MCF-7
8_a	16.2 \pm 2.4	7.98 \pm 2.4	25.61 \pm 1.3	–
8_b	10 \pm 2.4	18.01 \pm 2.3	26 \pm 1.3	–
8_d	7.23 \pm 2.1	7.12 \pm 2.0	70.17 \pm 2	–
9_a	–	9.26 \pm 2.4	–	42 \pm 1.2
12_b	–	–	86.26 \pm 2.2	–
Erlotinib	6.53 \pm 0.82	11.05 \pm 1.07	5.47 \pm 0.3	4.21 \pm 0.62

^aAll IC₅₀ values are calculated as the mean of at least three different experiments.

**Figure 4.** SAR according to modifiable moieties in the target compounds.

apoptotic effects through the caspase pathway^{69,70}. Here, the effect of the most active EGFR inhibitor **8a** on caspase-3 was examined in PC-3 cells. Compound **8a** was applied on PC-3 cells at a concentration of 3.04 μM for 24 h. The results revealed that such a compound generated a marked increase in the level of caspase-3 (452.3 pg/mL, 5.3-fold) compared to the control cells (84.24 pg/mL). In addition, the tested compound showed a comparable effect with the reference compound; staurosporine (413.1 pg/mL; Table 4 and Supplementary data).

2.3. Docking studies

To confirm our rationale of design, the binding modes of the synthesised compounds were investigated against the proposed

Table 3. *In vitro* enzymatic inhibitory activities against EGFR^{L858R} and EGFR^{T790M}.

Comp.	EGFR ^{WT} IC ₅₀ (μM) ^a	EGFR ^{T790M} IC ₅₀ (μM) ^a
8a	0.099 \pm 0.007	0.123 \pm 0.010
8d	0.419 \pm 0.029	0.290 \pm 0.023
9a	0.594 \pm 0.042	0.571 \pm 0.046
Erlotinib	0.043 \pm 0.003	0.071 \pm 0.006

^aThe results were presented as Mean \pm Standard error (SE) of three different tests.

targets using a docking approach. The used biological targets in docking studies were EGFR-TK Wild-type (EGFR^{WT}, PDB: 4HJO)⁷¹ and EGFR-TK mutant type (EGFR^{T790M}, PDB: 3W2O)⁷² using MOE 14.0 software. The co-crystallised ligands were used as reference molecules. The output of docking studies showed a high affinity of the synthesised compounds against the two tested targets compared to the reference molecules (Table 5).

To validate the docking procedures, the co-crystallised ligands (Erlotinib and TAK-285) were re-docked against EGFR^{WT} and EGFR^{T790M}, respectively. The RMSD of docked and original ligands of erlotinib and TAK-285 were 0.88 and 1.05 \AA , respectively. These values indicate the validity of the docking protocol (Figures 7 and 8).

The co-crystallised ligand (erlotinib) of EGFR^{WT} showed a binding energy of -22.12 kcal/mol. The heterocyclic system (quinazoline moiety) was buried in the adenine pocket forming a hydrogen bond with Met769. Also, it formed four hydrophobic interactions with Lue694, Ala719, and Leu820. The ethynylphenyl moiety was oriented into the hydrophobic pocket I forming three hydrophobic interactions with Ala719, Val702, and Lys721. The 2-methoxyethoxy groups occupied the hydrophobic region II forming a hydrogen bond with Cys773 (Figure 9).

Compound **8a** showed a binding mode like that of erlotinib with a binding energy of -19.29 kcal/mol. The 5H-pyrido[2',3':4,5]pyrimido[2,1-b]quinazoline-5,7(12H)-dione moiety

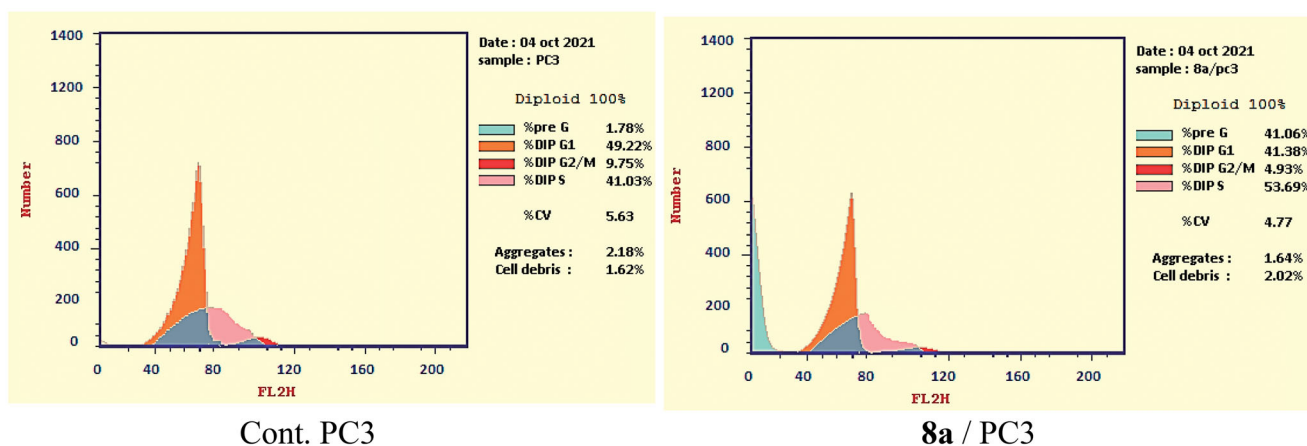


Figure 5. PC3 distribution upon treatment with compound **8a**.

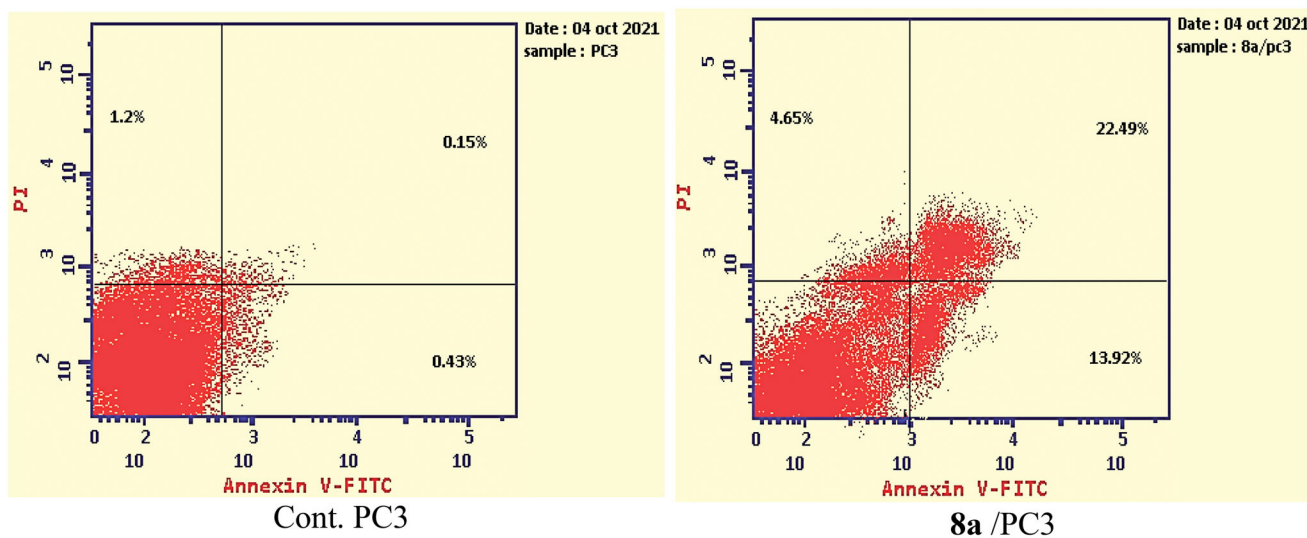


Figure 6. Apoptosis and necrosis percent induced by compound **8a**.

Table 4. Effect of compound **8a** on active caspase-3 in PC-3 cells after 24 h treatment.

Sample	Caspase-3 (pg/mL) ^a
8a /PC-3	452.3 ± 10.5
Staurosporine/PC-3	413.1 ± 11.66
Cont. (PC-3)	84.24 ± 16.5

^aValues are given as mean ± SEM of three independent experiments.

Table 5. The docking binding free energies of the synthesised compounds against EGFR^{WT} and EGFR^{T790M}.

Comp.	Binding free energy (kcal/mol)	
	EGFR ^{WT}	EGFR ^{T790M}
7a	-16.16	-11.59
7b	-16.61	-11.77
7c	-19.17	-15.03
7d	-21.41	-16.26
7e	-22.42	-19.57
8a	-19.29	-15.63
8b	-19.06	-18.13
8c	-21.92	-19.40
8d	-21.92	-19.30
9a	-15.80	-12.15
9b	-16.62	-15.14
9c	-19.23	-15.18
9d	-21.55	-17.63
9e	-22.46	-17.63
10a	-17.13	-15.27
10b	-19.19	-15.20
10c	-21.28	-16.57
10d	-22.48	-19.86
11a	-17.02	-14.22
11b	-16.92	-15.58
11c	-19.28	-15.89
11d	-21.60	-17.33
11e	-22.32	-19.22
12a	-20.96	-18.50
12b	-21.02	-20.62
12c	-21.67	-21.70
12d	-23.46	-22.39
Erlotinib	-22.12	-
TAK-285	-	-18.70

occupied the adenine pocket of the EGFR^{WT} forming one hydrogen bond with the crucial amino acid Met769. In addition, it formed nine hydrophobic interactions with Val702, Leu694, and Leu820. The tolyl moiety occupied the hydrophobic pocket I forming four hydrophobic interactions with Leu890, Ala719, and Lys721. Moreover, the 4-chlorophenyl moiety occupied the hydrophobic region II forming two hydrophobic interactions with Val702 and Arg817 (Figure 10).

Compound **8b** showed a binding energy of -19.06 kcal/mol. The 5H-pyrido[2',3':4,5]pyrimido[2,1-b]quinazoline-5,7(12H)-dione moiety was buried in the adenine pocket forming two hydrogen bonds with acid Met769 and Cys773. In addition, it formed six hydrophobic interactions with Val702, Leu694, and Leu820. The 4-methoxyphenyl moiety occupied pocket I forming two hydrophobic interactions with Val702, and Cys773. Moreover, the 4-chlorophenyl moiety occupied the hydrophobic II forming three hydrophobic interactions with Val721 and Ala719 (Figure 11).

With regard to compound **8d**, it showed a binding mode similar to the reference molecules with a binding energy of -21.92 kcal/mol. The 5H-pyrido[2',3':4,5]pyrimido[2,1-b]quinazoline-5,7(12H)-dione moiety was involved in two hydrogen bonds with the amino acids Met769 and Cys773 in the adenine pocket. In addition, it formed eight hydrophobic interactions with Val702,

Leu694, Gly772, and Leu820. The 3,4,5-trimethoxyphenyl moiety occupied pocket I forming two hydrophobic interactions with Ala719 and Leu820. It formed two hydrogen bonds with Thr766 and Thr830. Moreover, the tolyl moiety occupied the hydrophobic II forming three hydrophobic interactions with Val702, Arg817 and Cys773 (Figure 12).

Compound **9a** showed a binding energy of -15.80 kcal/mol. The 2-hydrazinylpyrido[2,3-d]pyrimidin-4(3H)-one moiety was inserted in the adenine pocket forming a hydrogen bond with the amino acid Met769. Further, it formed five hydrophobic interactions with Val702, Leu694, and Leu820. The 4-chlorophenyl moiety occupied pocket I forming three hydrophobic interactions with Leu764, Lys721, and Ala719. Moreover, the 2,4-dichlorophenyl moiety occupied the hydrophobic II forming five hydrophobic interactions with Val702, Arg817, Leu694, and Cys773 (Figure 13).

The synthesised compounds showed good binding affinities against EGFR^{T790M} with binding free energies ranging from -11.59 to -22.39 kcal/mol (Table 5). The co-crystallised ligand (TAK-285) exhibited a binding energy of -18.70 kcal/mol. The pyrrolo[3,2-d]pyrimidine moiety was buried in the adenine pocket forming a hydrogen bond with Met793 and three hydrophobic bonds with Leu844 and Ala743. The terminal 3-(trifluoromethyl)phenoxy group occupied the hydrophobic pocket I forming a hydrogen bond with Lys745. Also, it formed seven hydrophobic interactions with Lys745, Glu762, Leu788, and Ile759. In addition, the N-ethyl-3-hydroxy-3-methylbutanamide moiety occupied the hydrophobic region II forming hydrogen bond with Ser720. The phenyl moiety formed hydrophobic interactions with Met790, Val726, and Ala743 (Figure 14).

Compound **8c** exhibited a binding mode similar to that of TAK-285 with an affinity value of -19.40 kcal/mol. The 5H-pyrido[2',3':4,5]pyrimido[2,1-b]quinazoline-5,7(12H)-dione moiety occupied the adenine pocket of forming five hydrophobic interaction with Lys745, Glu762, and Leu844. Also, it formed three hydrogen bonds with Thr854, Met790, and Lys745. The 3,4,5-trimethoxyphenyl moiety occupied the hydrophobic pocket I and 4-chlorophenyl moiety occupied the hydrophobic region II forming three hydrophobic bonds with Leu718, Leu844, and Leu792 (Figure 15).

Compound **9a** exhibited a binding energy of -12.15 kcal/mol. The 2-hydrazinylpyrido[2,3-d]pyrimidin-4(3H)-one moiety occupied the adenine pocket of forming four hydrophobic interaction with Lys745, Glu762, and Thr854. Also, it formed two hydrogen bonds with Glu762 and Met766. The 2,4-dichlorophenyl moiety occupied the hydrophobic pocket I and 4-chlorophenyl moiety occupied the hydrophobic region II forming six hydrophobic bonds with Val726, Met793, Ala743, Leu844 and Leu792 (Figure 16).

Compound **10d** exhibited a binding energy of -19.86 kcal/mol. The 1,2-dihydropyrido[2,3-d][1,2,4]triazolo[4,3-a]pyrimidine-3,5-dione moiety occupied the adenine pocket of forming three hydrogen bonds with Lys745, and Met790. Also, it formed four hydrophobic interactions with Lys745, and Met790. The 3,4,5-trimethoxyphenyl moiety occupied the hydrophobic pocket I and tolyl moiety occupied the hydrophobic region II forming three hydrophobic bonds with Leu718, Leu844 and Leu792 (Figure 17).

Compound **12d** exhibited a binding energy of -22.39 kcal/mol. The pyrido[2,3-d][1,2,4]triazolo[4,3-a]pyrimidin-5(1H)-one moiety occupied the adenine pocket of forming two hydrogen bonds with Gln791 and Met793. Also, it formed six hydrophobic interactions with Val726, Leu844, Ala743, and Met793. The 3,4,5-trimethoxyphenyl moiety occupied the hydrophobic pocket I and tolyl moiety occupied the hydrophobic region II forming three hydrophobic bonds with Leu788, Ile759 and Lys745 (Figure 18).

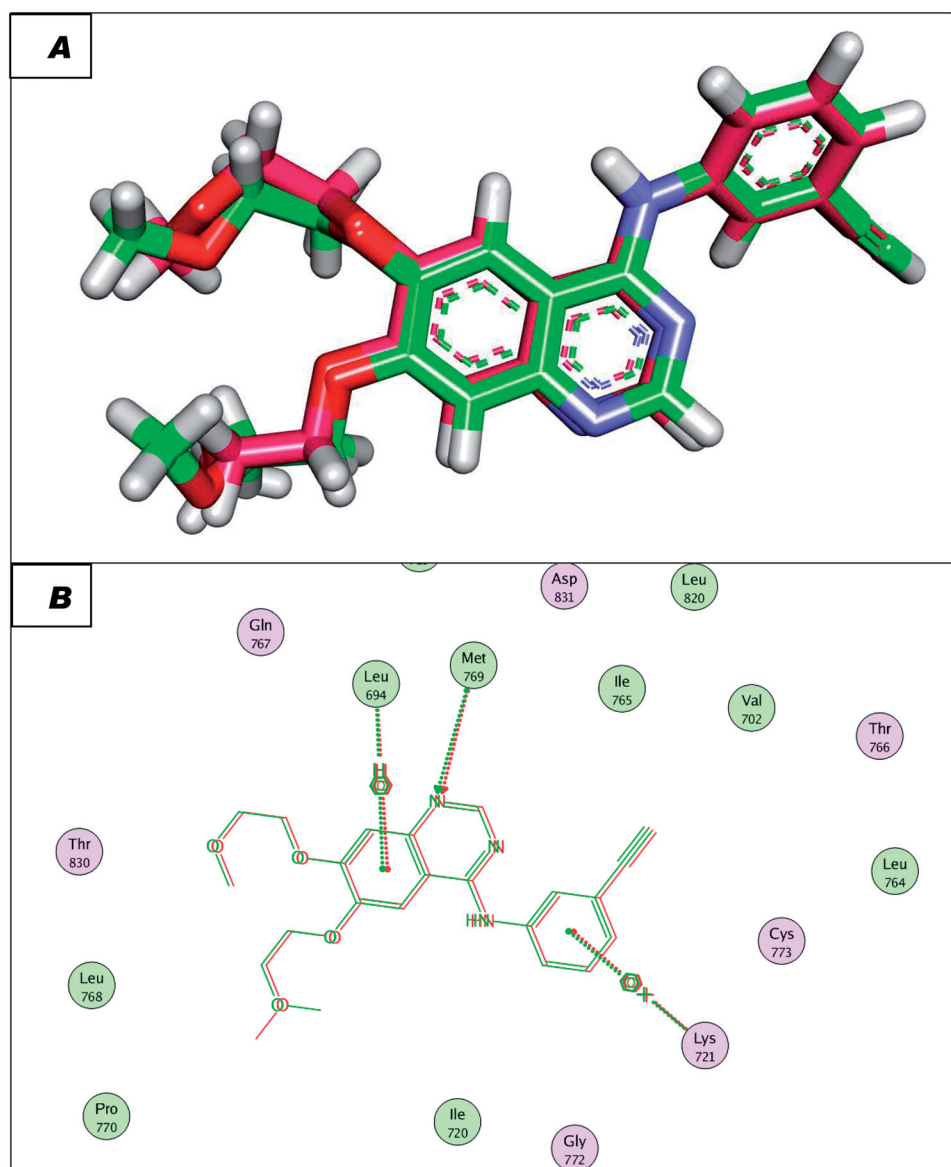


Figure 7. (A and B) 3D and 2D superimposition of the docked ligand (erlotinib; pink) and the original ligand (green) with RMSD value of 0.88 Å.

3. Conclusion

New nineteen pyrido[2,3-d]pyrimidin-4(3H)-one derivatives have been designed and synthesised as EGFR inhibitors. These compounds were evaluated for antiproliferative activities against A-549, PC-3, HCT-116, and MCF-7 cell lines. Compounds **8a**, **8b**, **8d**, **9a**, and **12b** exhibited the highest activities. Compound **8a** showed promising activities against A-549, PC-3, and HCT-116 cell lines with IC_{50} values of 16.2, 7.98, and 25.61 μ M, respectively. Compounds **8a**, **8b**, and **9a** showed promising inhibitory activities against EGFR^{WT} with IC_{50} values of 0.099, 0.419, and 0.594 μ M, respectively. In addition, such derivatives showed good inhibitory effects against EGFR^{T790M} with IC_{50} values of 0.123, 0.290, and 0.571 μ M, respectively. The most promising candidate **8a** induced a significant apoptotic effect in PC-3 cells and arrested the cell cycle at the pre-G1 phase. Structure-activity relationship studies revealed that tetracyclic 5H-pyrido [2',3':4,5]pyrimido[2,1-b]quinoxaline-5,7(12H)-dione derivatives **8a-d** have the preferred impact on the anticancer activity. In addition, the existence of an electron-donating (OCH₃) group at 4-position of compounds **8a** and **8d** is beneficial for activity. To give an additional comprehensive

investigation about the mechanism of action of the synthesised compounds, docking studies were performed against EGFR^{WT} and EGFR^{T790M}. Docking studies revealed that the synthesised compounds have similar binding modes against the prospective biological targets. This work introduces compounds **8a** as a potential promising EGFR inhibitor.

4. Experimental

4.1. Chemistry

4.1.1. General

All details of chemicals and different apparatus for analyses were provided in [Supplementary data](#).

4.1.2. General procedure for synthesis of thioxopyrimidinone **7a-e**

A mixture of the appropriate α , β -unsaturated ketones **6a-e** (0.01 mol) and 6-amino-2,3-dihydro-2-thioxopyrimidin-4(1H)-one (3) (1.43 g, 0.01 mol) was heated in dry DMF (20 ml) under reflux for

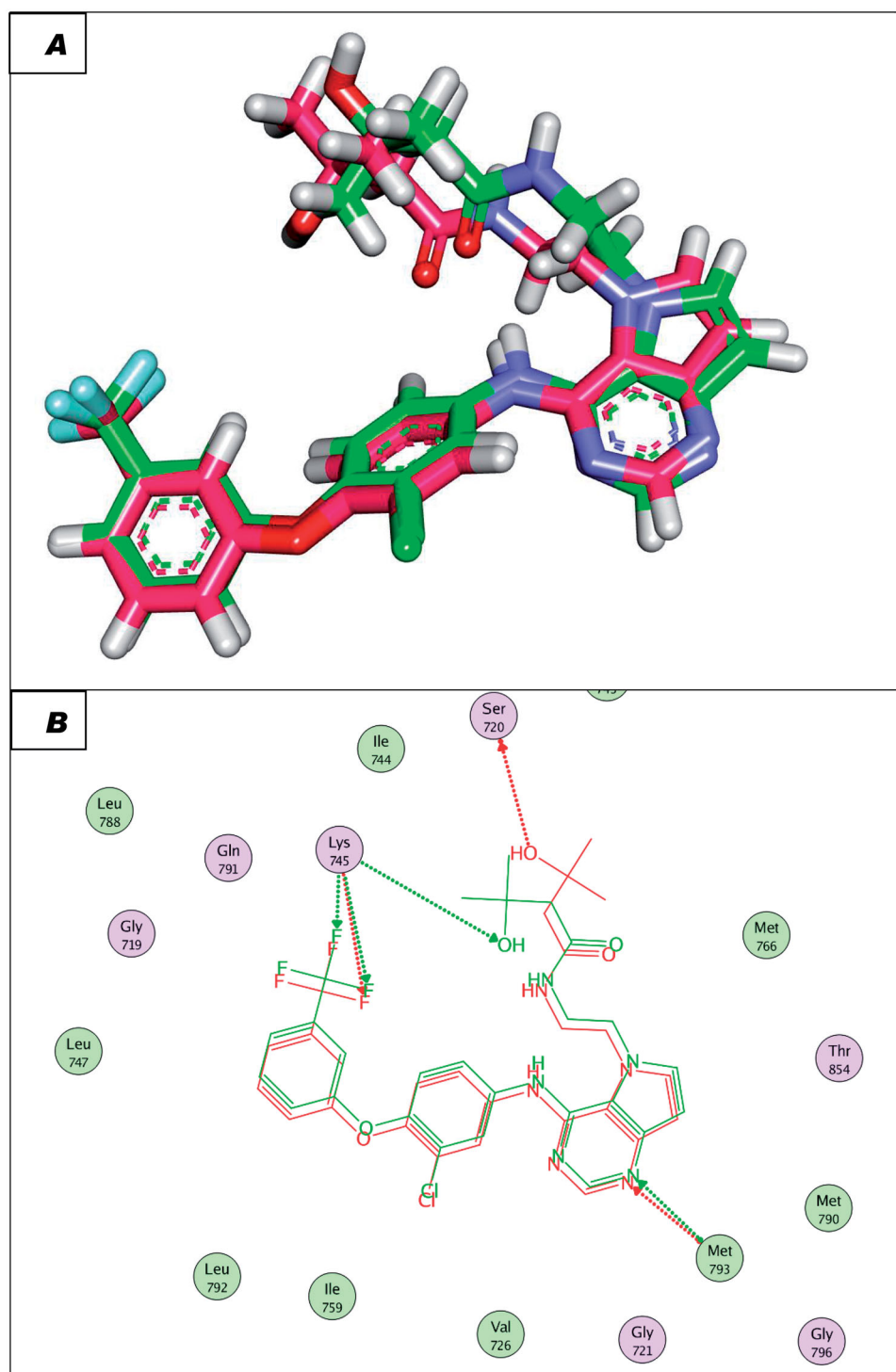


Figure 8. (A and B) 3D and 2D superimposition of the docked ligand of mutant EGFR (TAK-285; Pink) and the original ligand (green) with RMSD value of 1.06 Å.

10–15 h. After cooling, the precipitates were filtered and crystallised from DMF to afford compounds **7a–e**. All spectral data of thio-oxo derivatives **7b–e** was reported in our previous work⁷³. Herein, we described our newly synthesised thio-oxo precursor **7a**.

4.1.2.1. 7-(4-Chlorophenyl)-5-(2,4-dichlorophenyl)-2-thioxo-2,3-dihydropyrido [2,3-d]pyrimidin-4(1H)-one (7a). Yield (50%); m.p.

318–320 °C. IR (KBr) (cm^{-1}): 3387 (NH), 1701 (C=O); ¹HNMR (400 MHz, DMSO- d_6) δ (ppm): 7.40–7.76(m, 5H, Ar-H), 7.97 (s, 1H, pyridine-H6), 8.26 (d, $J = 8$ Hz, 2H, chlorophenyl-H2,H6), 12.50 (brs, 1H, NH, D₂O exchangeable); ¹³CNMR (DMSO- d_6) δ (ppm): 108.8, 118.5, 126.5, 127.7, 128.7, 129.1, 130.1, 132.4, 133.1, 134.7, 136.7, 149.3, 152.4, 158.3, 158.6, 162.2, 175.6; MS (m/z) 434; Anal. Calc. for: (C₁₉H₁₀Cl₃N₃OS): C, 52.50; H, 2.32; N, 9.67; Found: C, 52.57; H, 2.36; N, 9.73%.

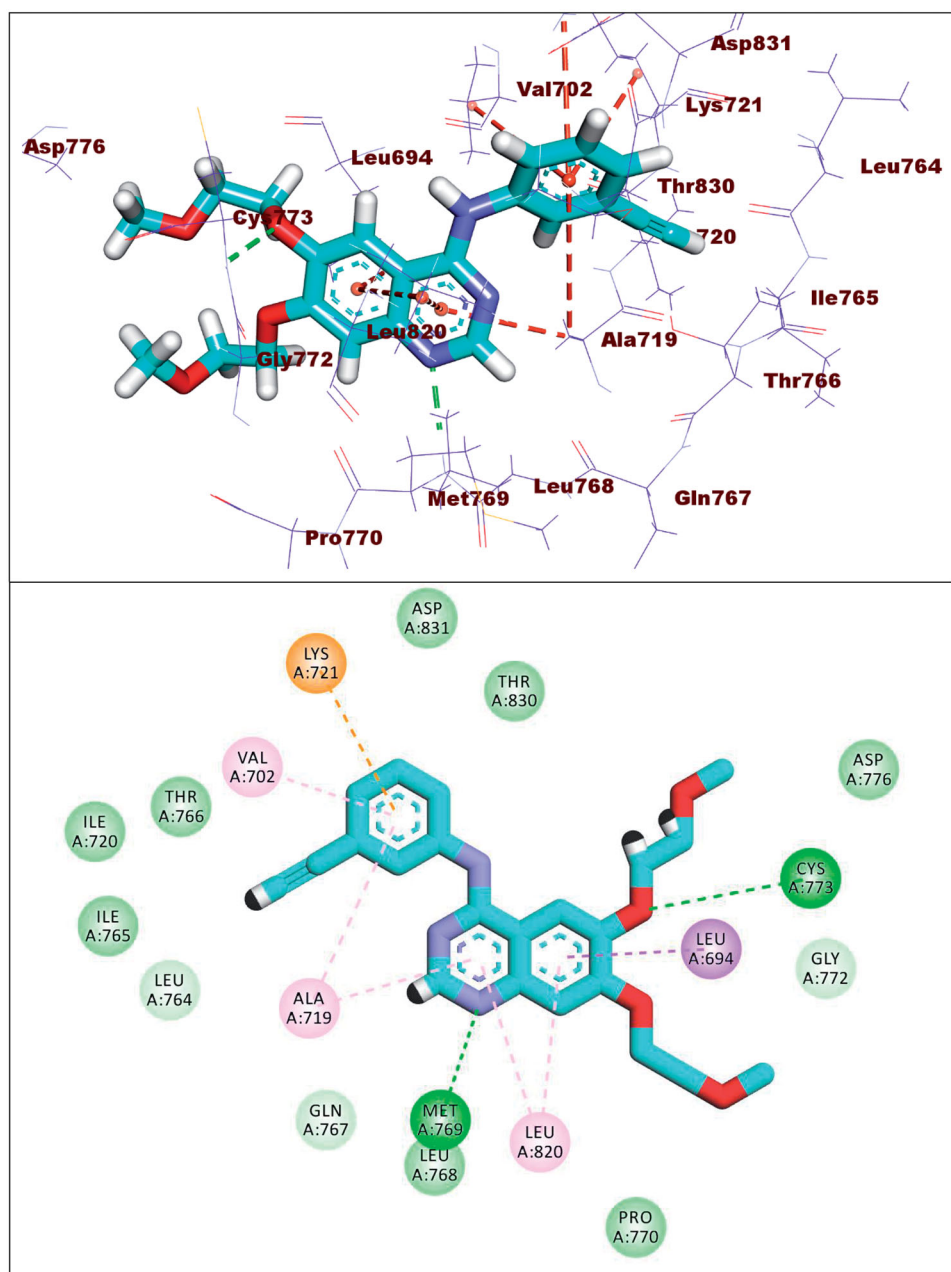


Figure 9. Erlotinib docked into the active site of EGFR^{WT}.

4.1.3. General procedure for synthesis of 2,4-diaryl-5Hpyrido [2',3':4,5] pyrimido[2,1-b]quinazoline-5,7(12H)-dione(8a-d)

A mixture of 2-thioxopyrido[2,3-d]pyrimidine derivatives **7a-e** (0.01 mol) and anthranilic acid (1.37 g, 0.01 mol) was heated under reflux for 20 h in the presence of 2% sodium ethoxide (20 ml). The reaction mixture was cooled, poured into ice cold water and acidified by diluted hydrochloric acid. The formed precipitate was filtered, washed several times with water, dried and washed with hot ethanol to give the compounds **8a-d**.

4.1.3.1. 2-(4-Chlorophenyl)-4-(p-tolyl)-5H-pyrido[2',3':4,5]pyrimido[2,1-b]quinazoline-5,7(12H)-dione (8a). Yield (68%); m.p. >300 °C. IR(KBr) (cm⁻¹): 3479 (NH), 1750 (C=O), 1685 (C=O); ¹HNMR (400 MHz, DMSO-d₆) δ (ppm): 2.36 (s, 3H, CH₃), 6.45 (m, 1H, Ar-H), 6.66 (d, *J*=8.4 Hz, 2H, Ar-H), 7.10 (t, *J*=8 Hz, 1H, Ar-H), 7.20 (d, *J*=8 Hz, 2H, Ar-H), 7.31(d, *J*=8 Hz, 2H, Ar-H), 7.50 (s, 1H,

C6-pyridine), 7.56 (d, *J*=8.4 Hz, 2H, Ar-H), 8.42 (d, *J*=8.4 Hz, 2H, Ar-H), 11.19 (brs, 1H, NH, D₂O exchangeable); ¹³CNMR (DMSO-d₆) δ (ppm): 21.3, 106.3, 114.5, 116.1, 118.4, 127.7, 128.6, 129.0, 129.3, 129.36, 129.6, 131.8, 132.6, 135.5, 136.0, 136.2, 137.4, 150.1, 153.6, 154.2, 157.9, 169.7, 169.8; MS (*m/z*): 466 (M+2), 464 (M⁺); Anal. Calc. for: (C₂₇H₁₇ClN₄O₂): C, 69.75; H, 3.69; N, 12.05; % Found: C, 69.82; H, 3.74; N, 12.11%.

4.1.3.2. 4-(4-Methoxyphenyl)-2-(p-tolyl)-5H-pyrido[2',3':4,5]

pyrimido[2,1-b]quinazoline-5,7(12H)-dione (8b). Yield (52%); m.p. >300 °C. IR (KBr) (cm⁻¹): 3410 (NH), 1693 (C=O), 1750 (C=O); ¹HNMR (400 MHz, DMSO-d₆) δ (ppm): 2.36 (s, 3H, CH₃), 3.79 (s, 3H, OCH₃), 6.92–6.95 (m, 2H, Ar-H), 7.29–7.44 (m, 6H, Ar-H), 7.49 (s, 1H, C-6 pyridine), 8.07–8.10 (m, 4H, Ar-H), 11.11 (brs, 1H, NH, D₂O exchangeable); ¹³CNMR (DMSO-d₆) δ (ppm): 21.3, 55.6, 106.3, 114.5, 116.2, 118.7, 127.3, 128.1, 129.3, 129.3, 129.6, 131.4, 132.2,

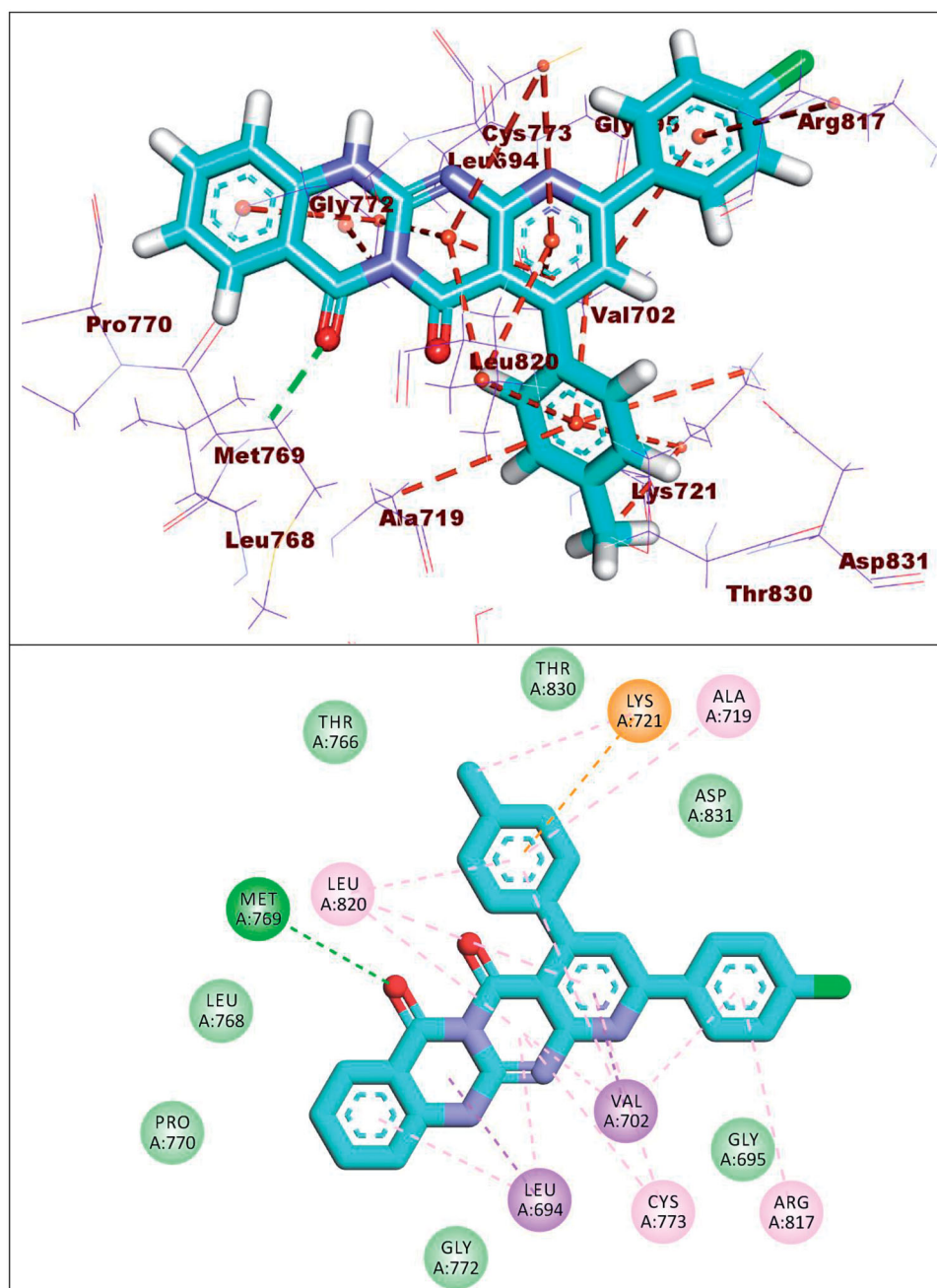


Figure 10. Compound **8a** docked into the active site of EGFR^{WT}.

135.4, 136.8, 136.2, 137.8, 150.2, 153.7, 154.8, 154.5, 157.6, 169.7, 169.8; MS (*m/z*): 460; Anal. Calc. for: (C₂₈H₂₀N₄O₃); C, 73.03; H, 4.38; N, 12.17%; Found: C, 73.07; H, 4.44; N, 12.23%.

4.1.3.3. 2-(4-Chlorophenyl)-4-(3,4,5-trimethoxyphenyl)-5H-pyrido[2',3':4,5] pyrimido[2,1-b]quinazoline-5,7(12H)-dione (8c). Yield (87%); m. p. <300 °C. IR (KBr) (cm⁻¹): 3468 (NH), 1708 (C=O); ¹HNMR (400 MHz, DMSO-d₆) δ (ppm): 3.74 (s, 3H, OCH₃), 3.80 (s, 6H, 2OCH₃), 6.51 (t, 1H, Ar-H), 6.74 (d, *J* = 8 Hz, 2H, Ar-H), 7.23 (m, 1H, Ar-H), 7.62–7.68 (m, 2H, Ar-H), 7.76 (s, 1H, C-pyridine), 8.32 (d, *J* = 8 Hz, 4H, Ar-H), 11.24 (brs, 1H, NH, D₂O exchangeable); ¹³CNMR (DMSO-d₆) δ (ppm): 56.6, 60.6, 106.3, 106.7, 109.0, 115.0, 119.6, 126.9, 129.3, 129.6, 129.9, 130.4, 131.5, 133.9, 134.2, 135.6, 137.9,

150.5, 152.5, 153.4, 157.8, 159.1, 161.4, 170.6; MS (*m/z*): 542 (M + 2), 540 (M⁺); Anal. Calc. for: (C₂₉H₂₁ClN₄O₅); C, 64.39; H, 3.91; N, 10.36%; Found: C, 64.44; H, 3.95; N, 10.41%.

4.1.3.4. 2-(p-Tolyl)-4-(3,4,5-trimethoxyphenyl)-5H-pyrido[2',3':4,5] pyrimido[2,1-b]quinazoline-5,7(12H)-dione (8d). Yield (57%); m.p. >300 °C. IR (KBr) (cm⁻¹): 3421 (NH), 1697(C=O); ¹HNMR (400 MHz, DMSO-d₆) δ (ppm): 2.39 (s, 3H, CH₃), 3.74 (s, 3H, OCH₃), 3.80 (s, 6H, 2OCH₃), 6.75 (s, 2H, Ar-H), 7.21–6.76 (m, 2H, Ar-H), 7.35 (d, *J* = 8 Hz, 2H, Ar-H), 7.46 (s, 1H, C6-pyridine), 7.57 (m, 2H, Ar-H), 7.99 (d, *J* = 8 Hz, 1H, Ar-H), 8.14 (d, *J* = 8 Hz, 1H, Ar-H), 11.65 (brs, 1H, NH, D₂O exchangeable); ¹³C NMR (DMSO-d₆) δ (ppm): 21.6, 56.2, 60.2, 106.0, 106.3, 106.7, 118.0, 127.9, 128.6, 129.3, 129.3,

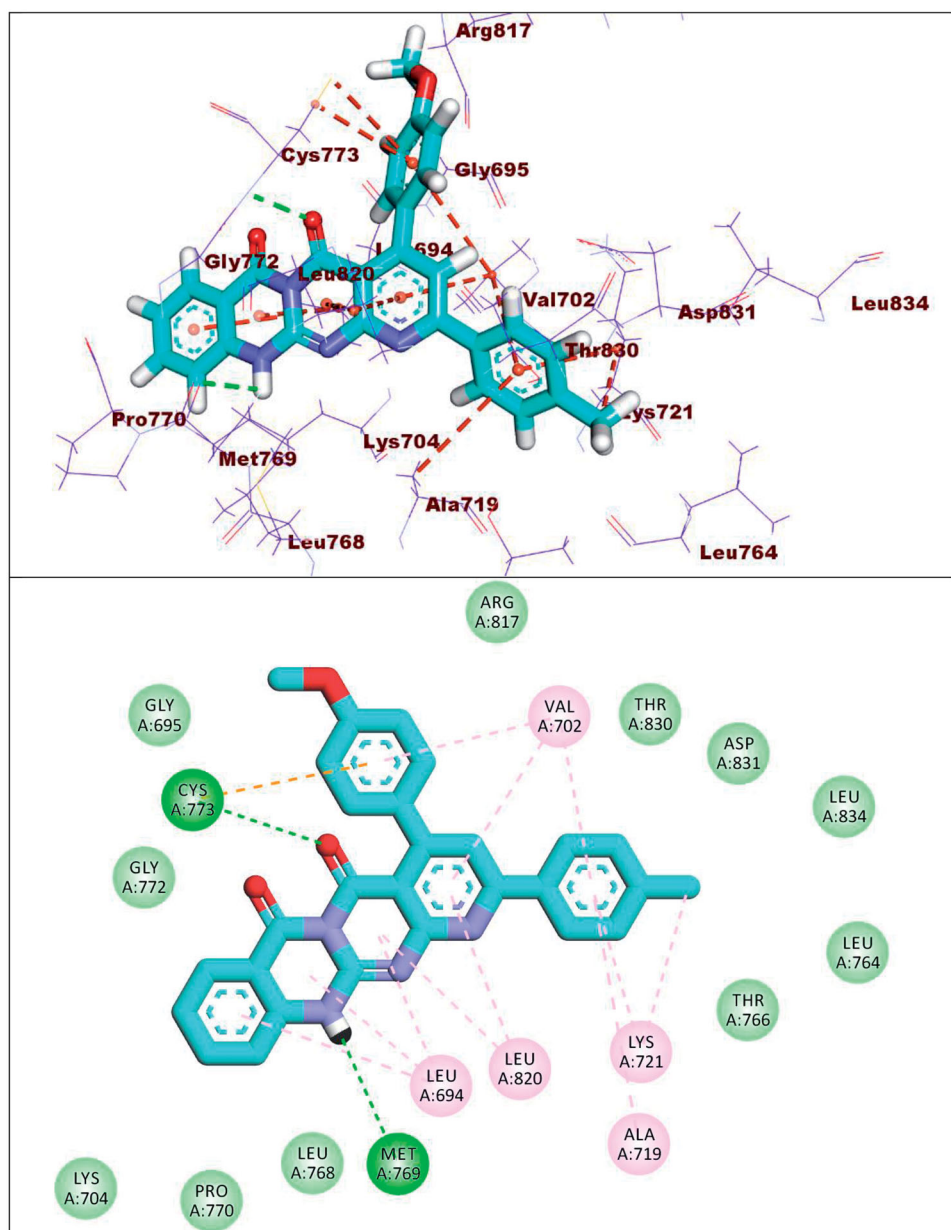


Figure 11. Compound **8b** docked into the active site of EGFR^{WT}.

129.6, 129.9, 134.2, 134.6, 136.5, 137.9, 140.9, 144.2, 150.1, 152.2, 153.4, 154.1, 159.1, 161.4, 169.4; MS (*m/z*): 520; Anal. Calc. for: (C₃₀H₂₄N₄O₅); C, 69.22; H, 4.65; N, 10.76%; Found: C, 69.25; H, 4.71; N, 10.82%.

4.1.4. General procedure for synthesis of 2-Hydrazinyl -5,7-diaryl-pyrido[2,3-d]pyrimidin-4(3H)-one (**9a–e**)

A mixture of 2-thioxopyrido[2,3-d]pyrimidine derivatives **7a–e** (0.004 mol) and hydrazine hydrate (99%, 3 ml, 0.006 mol) was heated under reflux in absolute ethanol (20 ml) for 10–15 h. After cooling, the precipitate was filtered and washed with hot ethanol to give compounds **9a–e**. All spectral data of hydrazino derivatives **9b–e** was reported in our previous work⁷³. Herein we described our newly synthesised hydrazine precursor **9a**.

4.1.4.1. 7-(4-Chlorophenyl)-5-(2,4-dichlorophenyl)-2-hydrazineyl-pyrido[2,3-d]pyrimidin-4(3H)-one **9a**. Yield (45%); m.p. 265–267 °C.

IR (KBr) (cm⁻¹): 3398, 3367 (NH) and (NH₂), 1685 (C=O); ¹H NMR (400 MHz, DMSO-d₆) δ (ppm): 7.59 (d, *J* = 8 Hz, 2H, Ar-H), 7.61–7.62 (m, 3H, Ar-H), 8.09 (s, 1H, H6-pyridine), 8.23 (brs, 2H, NH₂, D₂O exchangeable), 8.47 (d, *J* = 8 Hz, 2H, Ar-H), 9.18 (brs, 1H, NH, D₂O exchangeable), 12.83, (brs, 1H, NH, D₂O exchangeable); ¹³C NMR (DMSO-d₆) δ (ppm): 106.5, 112.8, 120.3, 124.7, 129.0, 129.2, 130.1, 131.6, 132.9, 136.14, 136.19, 144.7, 147.8, 148.6, 157.9, 160.1, 174.6; MS (*m/z*): 438 (M + 6), 436 (M + 4), 434 (M + 2), 432 (M⁺). Anal. Calc. for: (C₁₉H₁₂Cl₃N₅O); C, 52.74; H, 2.80; N, 16.19%; Found: C, 52.78; H, 2.86; N, 16.25.

4.1.5. General procedure for synthesis of 6,8-diaryl-pyrido[2,3-d][1,2,4]triazolo[4,3-a]pyrimidine-3,5-dione (**10a–d**)

A mixture of 2-hydrazinylpyrido[2,3-d]pyrimidine **9b–e** (1 mmol) and ethyl chloroformate (0.22 g, 2 mmol) in dry pyridine (10 ml) was heated under reflux for 9 h⁶⁰. The reaction mixture was cooled and the obtained solid was filtered, washed with ethanol, dried, and crystallised from DMF: EtOH (1:2).

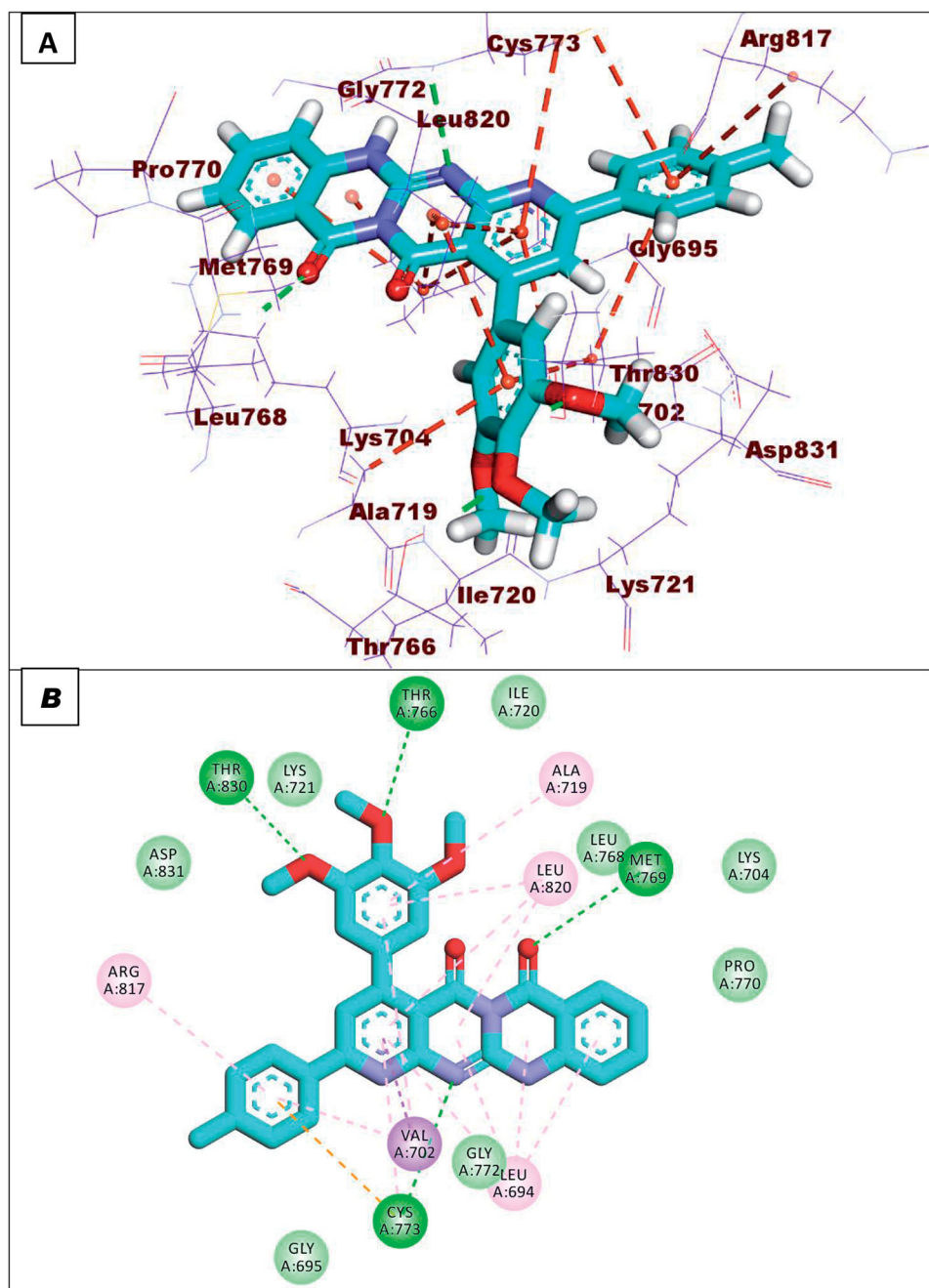


Figure 12. Compound **8d** docked into the active site of EGFR^{WT}.

4.1.5.1. 8-(4-Chlorophenyl)-6-(*p*-tolyl)-1,2-dihydropyrido[2,3-*d*][1, 2, 4]triazolo[4,3-*a*]pyrimidine-3,5-dione (10a). Yield (80%); m.p. 347–349 °C. IR (KBr) (cm⁻¹): 3383 (NH), 1685 (C=O), 1647 (C=O); ¹HNMR (400 MHz, DMSO-*d*₆) δ (ppm): 2.37 (s, 3H, CH₃), 7.24–7.26 (m, 3H, Ar-H), 7.37 (d, *J* = 8 Hz, 1H, Ar-H), 7.48–7.62 (m, 4H, 2Ar-H + 2NH, D₂O exchangeable), 7.92 (s, 1H, C-6pyridine), 8.48 (d, *J* = 8 Hz, 1H, Ar-H), 8.67 (d, *J* = 8 Hz, 1H, Ar-H); ¹³C NMR (DMSO-*d*₆) δ (ppm): 21.2, 108.6, 121.5, 128.1, 128.8, 129.4, 129.8, 134.5, 134.8, 135.7, 137.8, 145.7, 147.4, 148.0, 155.7, 159.4, 169.9; MS (*m/z*): 405 (M + 2), 403 (M⁺); Anal. Calc. for: (C₂₁H₁₄ClN₅O₂): C, 62.46; H, 3.49; N, 17.34%; Found: C, 62.54; H, 3.55; N, 17.40%.

4.1.5.2. 6-(4-Methoxyphenyl)-8-(*p*-tolyl)-1,2-dihydropyrido[2,3-*d*][1, 2, 4]triazolo[4,3-*a*]pyrimidine-3,5-dione (10b). Yield (54%); m.p.

366–368 °C. IR(KBr) (cm⁻¹): 3398 (NH), 3375 (NH), 1697 (C=O), 1654 (C=O); ¹HNMR (400 MHz, DMSO-*d*₆) δ (ppm): 2.38 (s, 3H, CH₃), 3.83 (s, 3H, OCH₃), 6.96 (d, *J* = 8 Hz, 2H, Ar-H), 7.32–7.40 (m, 5H, Ar-H), 7.79 (s, 1H, C6-pyridine), 8.06 (brs, 2H, 2NH, D₂O exchangeable), 8.57 (d, *J* = 8 Hz, 1H, Ar-H); MS (*m/z*): 399; Anal. Calc. for: (C₂₂H₁₇N₅O₃): C, 66.16; H, 4.29; N, 17.53%; Found: C, 66.24, H, 4.35; N, 17.60%.

4.1.5.3. 8-(4-Chlorophenyl)-6-(3,4,5-trimethoxyphenyl)-1,2-dihydropyrido[2,3-*d*][1, 2, 4]triazolo[4,3-*a*]pyrimidine-3,5-dione (10c). Yield (67%); m.p. 367–369 °C. IR(KBr) (cm⁻¹): 3160 (2NH), 1759, 1697(2C=O) ¹HNMR (400 MHz, DMSO-*d*₆) δ (ppm): 3.73 (s, 3H, OCH₃), 3.78 (s, 6H, 2OCH₃), 6.79 (s, 2H, Ar-H), 7.53–7.61 (m, 2H, Ar-H), 7.89 (s, 1H, C6-pyridine), 8.22–8.77 (m, 2H, Ar-H), 9.46 (s, 2H,

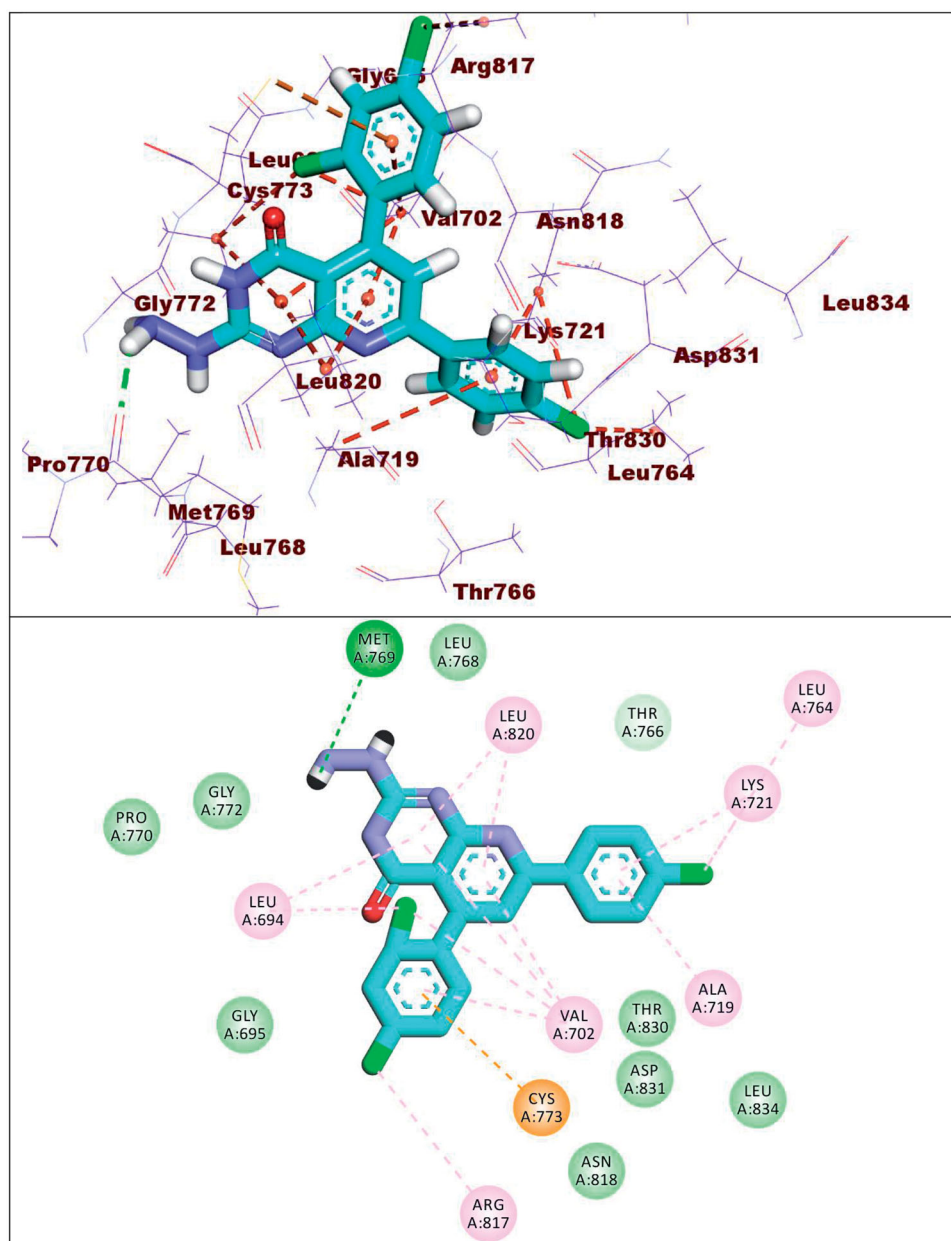


Figure 13. Compound **9a** docked into the active site of EGFR^{WT}.

2NH, D₂O exchangeable); ¹³C NMR (DMSO-d₆) δ (ppm); 56.1, 59.7, 105.7, 106.8, 116.4, 117.5, 119.1, 128.0, 129.6, 137.7, 140.5, 148.8, 149.4, 152.3, 155.8, 158.4, 161.9, 169.6; MS (*m/z*): 481 (*M* + 2), 479 (*M*⁺). Anal. Calc. for: (C₂₃H₁₈ClN₅O₅): C, 57.57; H, 3.78; N, 14.59%; Found: C, 57.64, H, 3.85; N, 14.64%.

4.1.5.4. 8-(*p*-Tolyl)-6-(3,4,5-trimethoxyphenyl)-1,2-dihydropyrido[2,3-*d*][1, 2, 4]triazolo [4,3-*a*]pyrimidine-3,5-dione (10d). Yield (54%); m.p. 391–393 °C. IR (KBr) (cm⁻¹): 3494 (NH), 3383 (NH), 1685 (C=O), 1660 (C=O); ¹H NMR (400 MHz, DMSO-d₆) δ (ppm): 2.37 (s, 3H, CH₃), 3.73 (s, 6H, 2 OCH₃), 6.73 (s, 2H, Ar-H), 7.34–7.45 (m, 2H, Ar-H), 7.95 (s, 1H, C6-pyridine), 8.07–8.11 (m, 2H, Ar-H), 9.26 (s, 1H, NH, D₂O exchangeable), 11.07 (s, 1H, NH, D₂O exchangeable); MS (*m/z*): 459. Anal. Calc. for: (C₂₄H₂₁N₅O₅): C, 62.74; H, 4.61; N, 15.24%; Found: C, 62.81, H, 4.67; N, 15.31%.

4.1.6. General procedure for 3-amino-6,8-diaryl-2,3-dihydropyrido[2,3-*d*][1, 2, 4]triazolo[4,3-*a*]pyrimidin-5(1H)-one 11(a-e)

A mixture of 2-hydrazinylpyrido[2,3-*d*]pyrimidines **9a-e** (0.002 mol) and ammonium thiocyanate (2.38 g, 0.3 mol) in glacial acetic acid (15 ml) was heated under reflux for 10 h. The reaction mixture was cooled, poured onto iced water and the precipitate was filtered, dried and washed with hot ethanol⁶⁰.

4.1.6.1. 3-Amino-8-(4-chlorophenyl)-6-(2,4-dichlorophenyl)-10,10a-dihydropyrido [2,3-*d*][1, 2, 4]triazolo[4,3-*a*]pyrimidin-5(1H)-one (11a). Yield (33%); m.p. 381–383 °C. IR (KBr) (cm⁻¹): 3421, 3356 (NH, NH₂), 1681 (C=O); ¹H NMR (400 MHz, DMSO-d₆) δ (ppm): 7.09 (brs, 1H, NH, D₂O exchangeable), 7.33 (brs, 2H, NH₂, D₂O exchangeable), 7.52–7.63 (m, 3H, Ar-H), 7.70 (d, *J* = 8 Hz, 1H, Ar-H), 7.85 (s, 1H, C6-pyridine), 8.04 (s, 1H, Ar-H), 8.28 (d, *J* = 12 Hz, 2H,

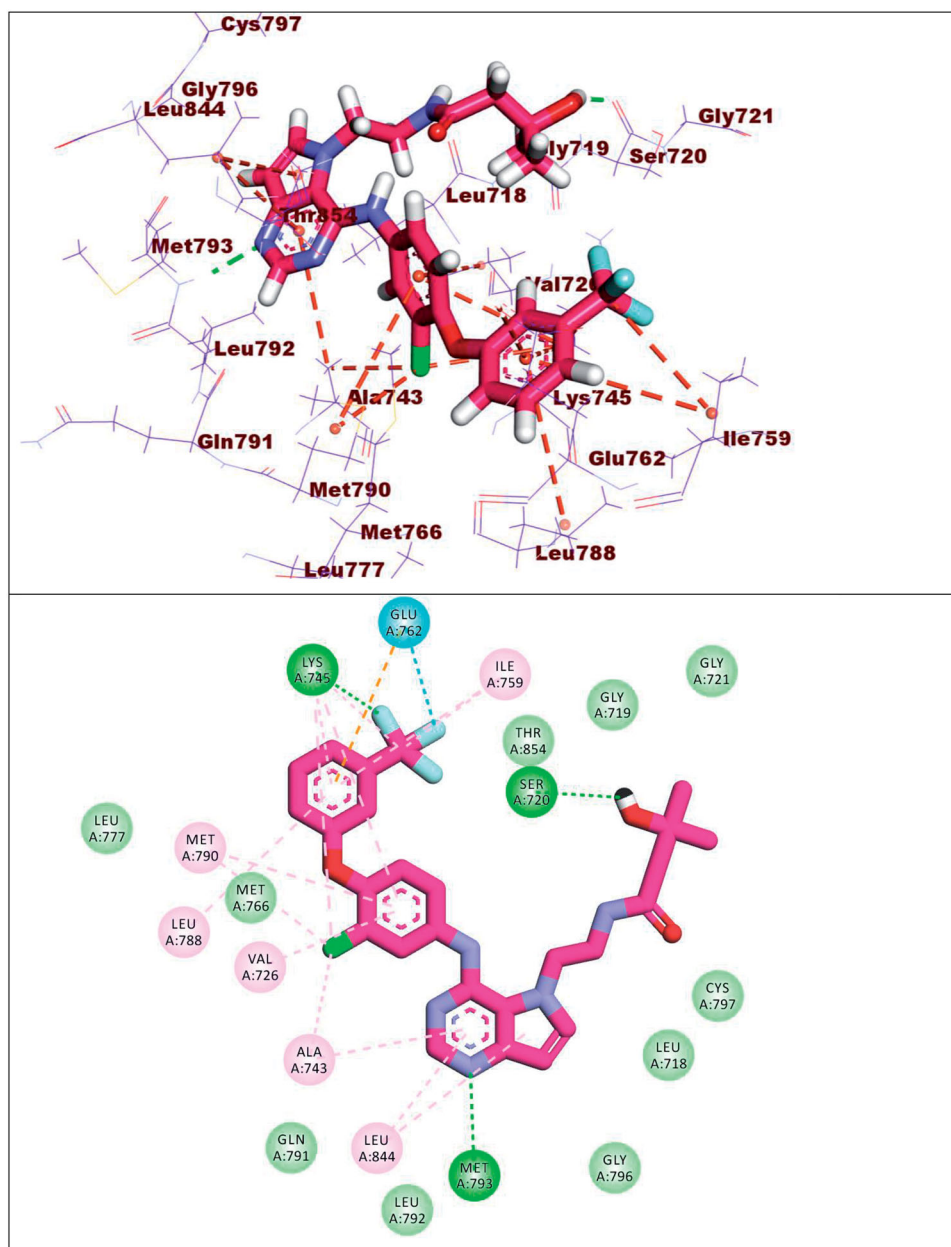


Figure 14. Co-crystallised ligand (TAK-285) docked into the active site of EGFR^{T790M}.

Ar-H); ¹³C NMR (DMSO-d₆) δ (ppm): 119.5, 127.4, 128.4, 129.1, 129.8, 131.0, 132.1, 132.4, 134.4, 134.7, 136.4, 136.7, 138.0, 141.1, 147.6, 148.5, 154.5, 167.2; MS (*m/z*): 463 (*M*+6), 461 (*M*+4), 459 (*M*+2), 457 (*M*⁺). Anal. Calc. for: (C₂₀H₁₁Cl₃N₆O); C, 52.48; H, 2.42; N, 18.36%; Found: C, 52.55; H, 2.47; N, 18.42%.

4.1.6.2. 3-Amino-8-(4-chlorophenyl)-6-(*p*-tolyl)-2,3-dihydropyrido[2,3-*d*][1, 2, 4] triazolo[4,3-*a*]pyrimidin-5(1*H*)-one (11b). Yield (33%); m.p. 383–385 °C. IR (KBr) (cm⁻¹): 3422, 3394 (NH, NH₂), 1697 (C=O); ¹H NMR (400 MHz, DMSO-d₆) δ (ppm): 2.34 (s, 3H, CH₃), 7.16–7.22 (m, 2H, Ar-H), 7.33 (d, *J*=8 Hz, 2H, Ar-H), 7.53–7.62 (d, *J*=8 Hz, 2H), 7.88 (s, 1H, C-6pyridine), 8.28 (d, *J*=8 Hz, 2H), 11.66 (brs, 1H, NH, D₂O exchangeable), 11.65, (brs, 2H, NH₂, D₂O exchangeable); ¹³C NMR (DMSO-d₆) δ (ppm): 20.6, 106.5, 109.3,

119.7, 122.7, 127.1, 128.3, 129.4, 134.7, 135.5, 137.4, 145.8, 147.3, 150.2, 153.7, 155.6, 167.4; MS (*m/z*): 404 (*M*+2), 402 (*M*⁺); Anal. Calc. for: (C₂₁H₁₅ClN₆O); C, 62.61; H, 3.75; N, 20.86%; Found: C, 62.66; H, 3.84; N, 20.91%.

4.1.6.3. 3-Amino-6-(4-methoxyphenyl)-8-(*p*-tolyl)-2,3-dihydropyrido[2,3-*d*][1, 2, 4] triazolo[4,3-*a*]pyrimidin-5(1*H*)-one (11c). Yield (47%); m.p. 381–383 °C. IR (KBr) (cm⁻¹): 3425, 4332 (NH, NH₂), 1697 (C=O); ¹H NMR (400 MHz, DMSO-d₆) δ (ppm): 2.35 (s, 3H, CH₃), 3.81 (s, 3H, OCH₃), 6.91–6.96 (m, 2H, Ar-H), 7.31–7.40 (m, 4H, Ar-H), 7.81 (s, 1H, C6-pyridine), 8.14 (d, *J*=8 Hz, 2H, Ar-H), 11.11 (brs, 2H, NH₂, D₂O exchangeable), 11.57 (brs, 1H, NH, D₂O exchangeable); ¹³C NMR (DMSO-d₆) δ (ppm): 21.2, 54.7, 112.8, 127.7, 129.4, 130.1, 133.4, 139.7, 140.7, 145.4, 145.7, 149.6, 150.0,

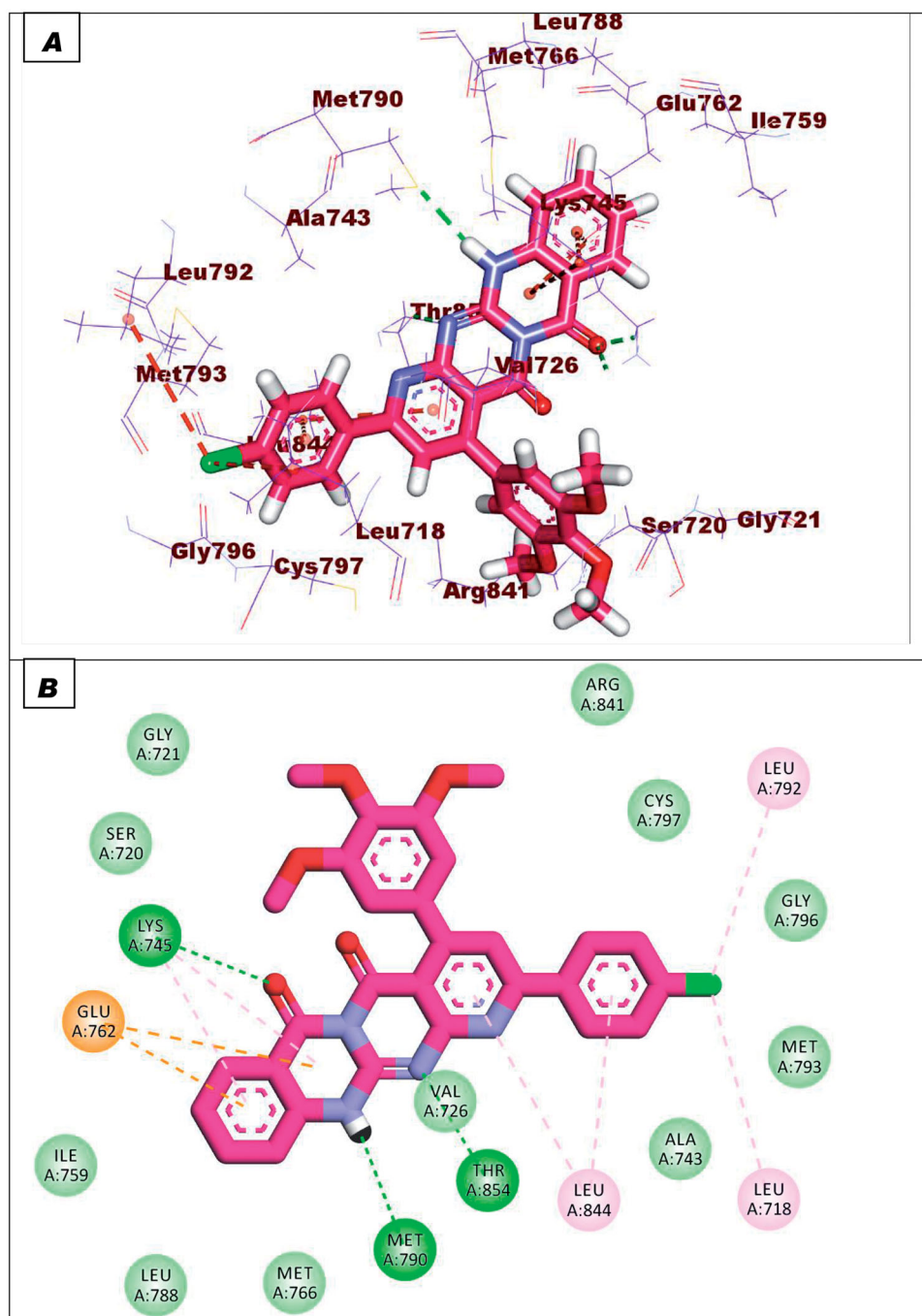


Figure 15. Binding of compound **8c** with EGFR^{T790M}.

153.3, 153.6, 159.3, 162.6, 167.9; MS (*m/z*): 398. Anal. Calc. for: (C₂₂H₁₈N₆O₂); C, 66.32; H, 4.55; N, 21.09%; Found: C, 66.36, H, 4.60; N, 21.14%.

4.1.6.4. 3-Amino-8-(4-chlorophenyl)-6-(3,4,5-trimethoxyphenyl)-2,3-dihydropyrido[2,3-d][1, 2, 4]triazolo[4,3-a]pyrimidin-5(1H)-one (11d). Yield (85%); m.p. 365–367 °C. IR (KBr) (cm⁻¹): 3437, 3425 (NH, NH₂), 1708 (C=O); ¹H NMR (400 MHz, DMSO-d₆) δ (ppm): 3.71 (s, 3H, OCH₃), 3.78 (s, 6H, 2OCH₃), 7.17 (s, 2H, Ar-H), 7.61–8 (m, 3H, Ar-H + C6-pyridine), 8.23–8.31 (m, 2H, Ar-H), 11.18 (brs, 2H, NH₂, D₂O exchangeable), 11.71 (brs, 1H, NH, D₂O exchangeable); ¹³C NMR (DMSO-d₆) δ (ppm): 56.0, 60.0, 106.4, 106.2, 128.8, 129.1, 129.4, 129.8, 134.1, 135.7, 140.7, 150.0, 151.7, 152.9, 153.6, 157.3,

160.9, 167.3; MS (*m/z*): 480 (M + 2), 478 (M⁺) Anal. Calc. for: (C₂₃H₁₉ClN₆O₄); C, 57.69; H, 4.00; N, 17.55%; Found: C, 57.74; H, 4.07; N, 17.59%.

4.1.6.5. 3-Amino-8-(p-Tolyl)-6-(3,4,5-trimethoxyphenyl)-2,3-dihydropyrido[2,3-d][1, 2, 4]triazolo[4,3-a]pyrimidin-5(1H)-one (11e). Yield (85%); m.p. 358–360 °C. IR (KBr) (cm⁻¹): 3433, 3367 (NH, NH₂), 1701 (C=O) ¹H NMR (400 MHz, DMSO-d₆) δ (ppm): 2.37 (s, 3H, CH₃), 3.77 (s, 3H, OCH₃), 3.78 (s, 6H, 2OCH₃), 6.73–6.78 (m, 2H, Ar-H), 7.32–7.39 (m, 2H, Ar-H), 7.92 (s, 1H, C6-pyridine), 8.19 (d, J = 8 Hz, 2H, Ar-H), 11.15 (brs, 2H, NH₂, D₂O exchangeable), 11.61 (s, 1H, NH, D₂O exchangeable); ¹³C NMR (DMSO-d₆) δ (ppm): 20.5, 55.7, 59.7, 106.5, 107.9, 114.8, 117.5, 127.5, 129.4, 134.1, 137.1,

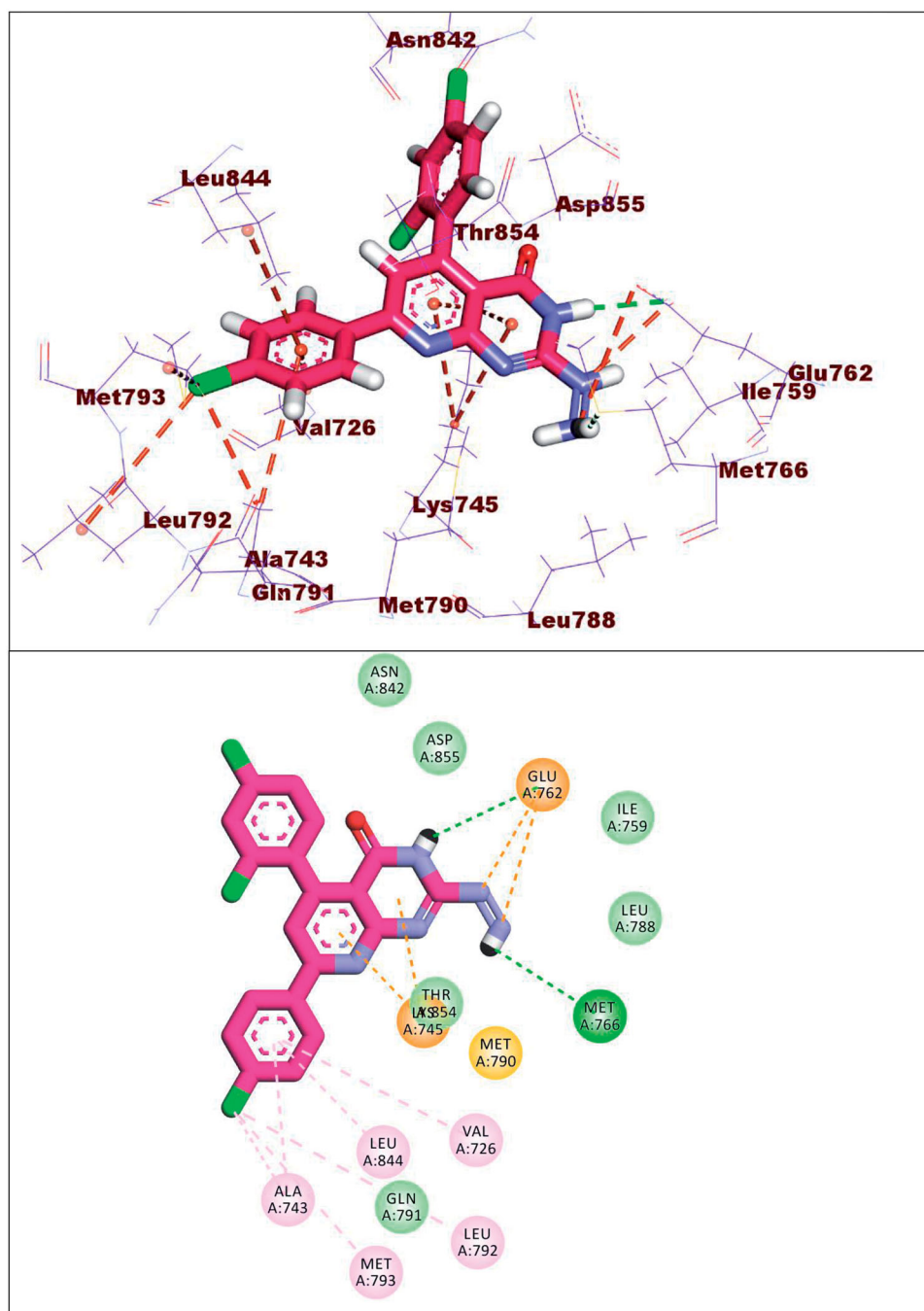


Figure 16. Binding of compound 9a with EGFR^{T790M}.

140.1, 150.0, 152.0, 153.4, 153.7, 158.6, 161.3, 167.7; MS (*m/z*): 458; Anal. Calc. for: (C₂₄H₂₂N₆O₄); C, 62.87; H, 4.84; N, 18.33%; Found: C, 62.94; H, 4.91; N, 18.39%.

4.1.6.6. 3-Phenyl-6,8-disubstitutedphenylpyrido[2,3-d][1, 2, 4]triazolo[4,3-a]pyrimidin-5(1H)-one (12a-e). To a solution of hydrazine derivative 9b-e (0.001 mol) in dry pyridine (20 ml) benzoyl chloride was added (0.001 mol), and the resulting mixture was heated under reflux for 10–15 h. After cooling, the formed precipitate was filtered washed with hot ethanol to afford 12a-d, respectively.

4.1.6.7. 8-(4-Chlorophenyl)-3-phenyl-6-(p-tolyl)pyrido[2,3-d][1, 2, 4]triazolo[4,3-a]pyrimidin-5(1H)-one (12a). Yield (67%); m.p.

315–317 °C. IR(KBr) (cm⁻¹): 3414(NH) 1750 (C=O); ¹H NMR (400 MHz, DMSO-d₆) δ (ppm): 2.40 (s, 3H, CH₃), 7.27–8.30 (m, 14H, Ar-H), 11.21(brs, 1H, NH, D₂O exchangeable); ¹³C NMR (DMSO-d₆) δ (ppm): 21.3, 106.3, 118.0, 128.2, 128.2, 128.6, 129.3, 135.5, 136.6, 136.9, 138.5, 142.2, 150.8, 151.5, 153.8, 154.1, 155.2, 158.1, 162.8, 166.1, 188.4; MS *m/z* (%): 465(M + 2), 463 (M⁺); Anal. Calc. for: (C₂₇H₁₈ClN₅O); C, 69.90; H, 3.91; N, 15.10%; Found: C, 69.97; H, 3.98; N, 15.14%.

4.1.6.8. 6-(4-Methoxyphenyl)-3-phenyl-8-(p-tolyl)pyrido[2,3-d][1, 2, 4]triazolo[4,3-a]pyrimidin-5(1H)-one (12b). Yield (33%); m.p. 325–327 °C. IR (KBr) (cm⁻¹): 3414, NH, 1720 (C=O); ¹H NMR (400 MHz, DMSO-d₆) δ (ppm); 2.39 (s, 3H, CH₃), 3.85 (s, 3H, OCH₃),

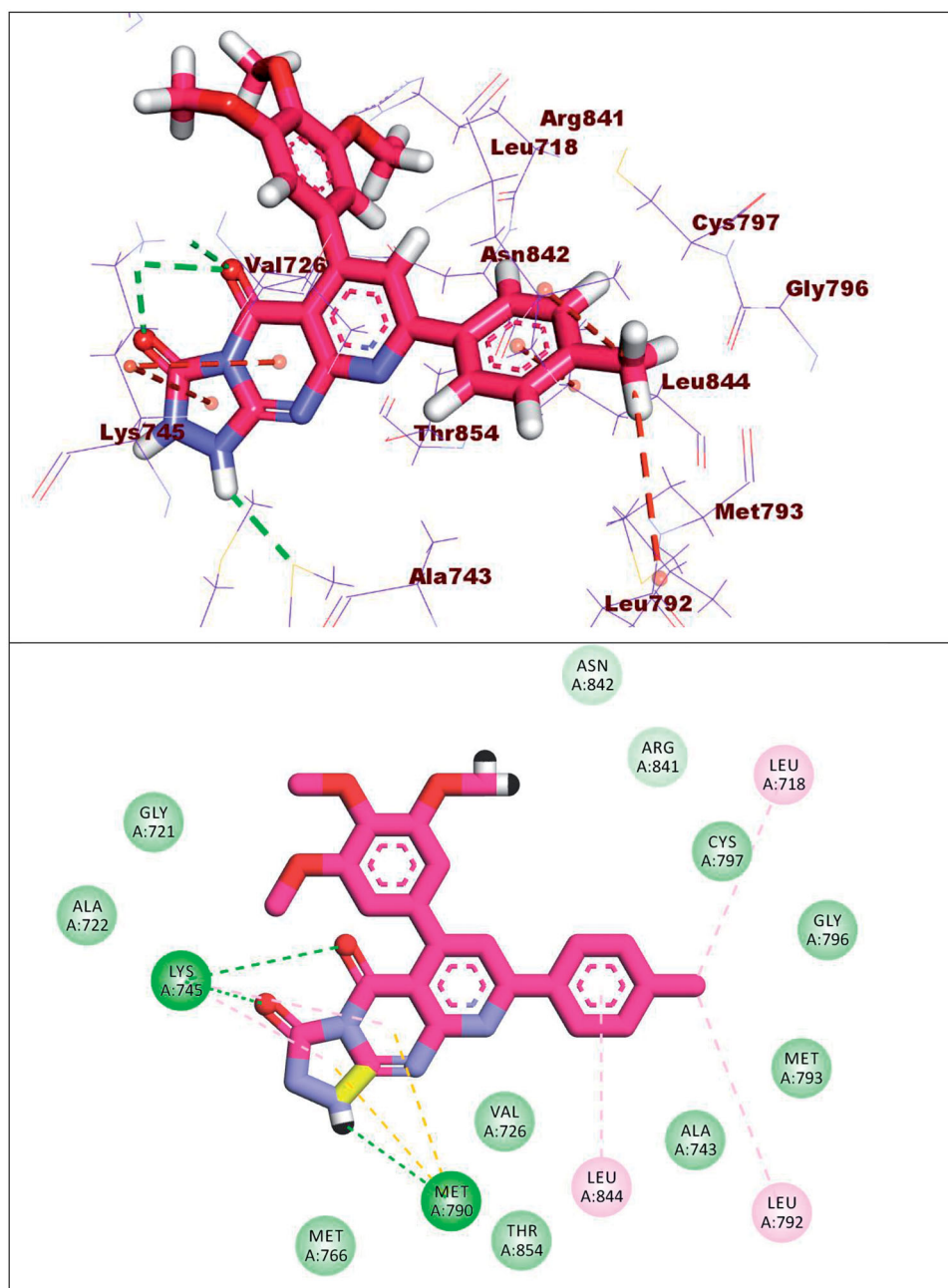


Figure 17. Binding of compound 10d with EGFR^{T790M}.

7.03–8.32 (m, 15H 14Ar-H + NH- D₂O exchangeable); ¹³C NMR (DMSO-d₆) δ (ppm): 21.6, 55.5, 113.2, 127.1, 127.6, 128.5, 129.0, 129.5, 129.8, 129.9, 130.3, 130.9, 131.5, 132.7, 135.4, 143.6, 145.2, 150.4, 154.6, 158.4, 160.3, 170.6; MS (*m/z*): 459; Anal. Calc. for: (C₂₈H₂₁N₅O₂); C, 73.19; H, 4.61; N, 15.24%; Found: C, 73.25; H, 4.66; N, 15.27%.

4.1.6.9. 8-(4-Chlorophenyl)-3-phenyl-6-(3,4,5-trimethoxyphenyl)pyrido[2,3-d][1, 2, 4]triazolo[4,3-a]pyrimidin-5(1H)-one (12c). Yield (33%); m.p. 313–315 °C. IR (KBr) (cm⁻¹): 3417 (NH), 1693 (C=O); ¹H NMR (400 MHz, DMSO-d₆) δ (ppm): 3.7 (s, 3H, OCH₃), 3.8 (s, 6H, 2OCH₃), 7.47–5.9 (m, 3H, Ar-H), 7.59–7.63 (m, 4H, Ar-H), 7.93–8.06 (m, 3H, 2Ar-H + 1NH-D₂O exchangeable), 8.55–8.59 (m, 1H, C6-pyridine), 8.91–8.92 (m, 2H, Ar-H); ¹³CNMR (DMSO-d₆) δ (ppm): 55.6, 59.6, 113.3, 123.9, 127.2, 128.9, 129.3, 129.5, 129.7, 129.8,

129.9, 130.3, 130.9, 132.6, 143.3, 146.5, 152.7, 160.2, 169.2; MS (*m/z*): 541(M + 2), 539 (M⁺); Anal. Calc. for: (C₂₉H₂₂ClN₅O₄); C, 64.51; H, 4.11; N, 12.97%; Found: C, 64.57; H, 4.16; N, 13.03%.

4.1.6.10. 3-Phenyl-8-(*p*-tolyl)-6-(3,4,5-trimethoxyphenyl)pyrido[2,3-d][1, 2, 4]triazolo [4,3-a]pyrimidin-5(1H)-one(12d). Yield (33%); m.p. 322–324 °C. IR (KBr) (cm⁻¹): 3464 (NH), 1701 (C=O); ¹H NMR (400 MHz, DMSO-d₆) δ (ppm): 2.37 (s, 3H, CH₃), 3.75 (s, 3H, OCH₃), 3.9 (s, 6H, 2OCH₃), 6.76–7.07 (m, 2H, Ar-H), 7.09–7.87 (m, 8H, Ar-H), 8.10–8.22 (m, 2H, Ar-H), 11.16 (brs, 1H, NH, D₂O exchangeable); ¹³C NMR (DMSO-d₆) δ (ppm): 20.8, 56.1, 60.1, 105.5, 106.5, 107.9, 108.9, 117.5, 118.8, 120.4, 127.4, 128.4, 129.1, 130.5, 132.3, 133.8, 134.4, 137.1, 140.1, 150.0, 151.7, 153.3, 158.6, 162.6; MS (*m/z*): 519; Anal. Calc. for: (C₃₀H₂₅N₅O₄); C, 69.35; H, 4.85; N, 13.48%; Found: C, 69.41; H, 4.91; N, 13.52%.

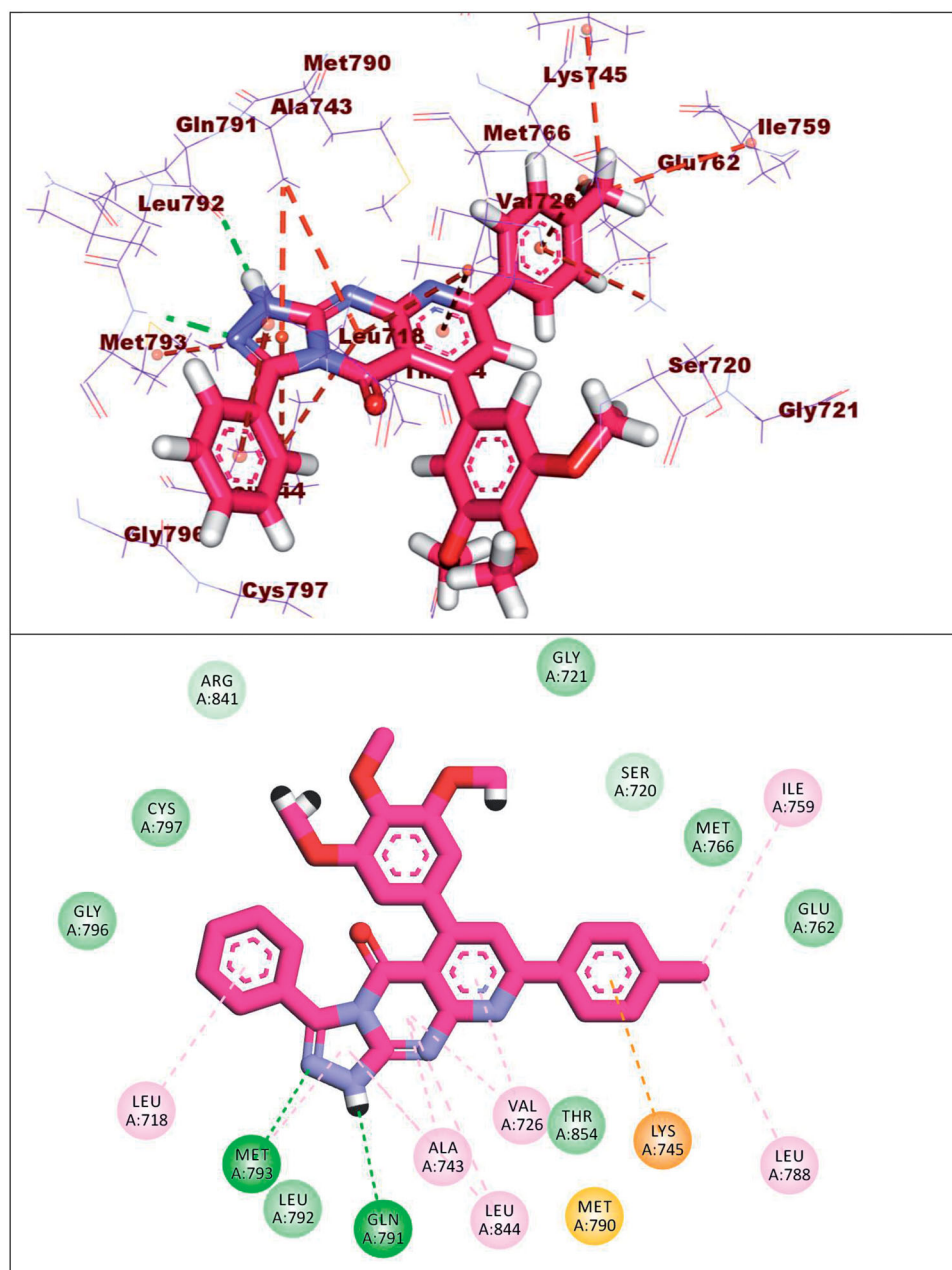


Figure 18. Binding of compound 12d with EGFR^{T790M}.

4.2. Biological evaluation

4.2.1. In vitro cytotoxic activity

In vitro cytotoxicity was carried out using MTT assay protocol⁶³ as described in Supplementary data.

4.2.2. In vitro EGFR kinase assay

In vitro EGFR inhibitory activity was assessed using Homogeneous time-resolved fluorescence (HTRF) assay⁶⁴ as described in Supplementary data.

4.2.3. Cell cycle analysis

The effect of compound **8a** on cell cycle distribution was performed using propidium iodide (PI) staining technique as described in Supplementary data^{65,74,75}.

4.2.4. Apoptosis analysis

The effect of compound **8a** on cell apoptosis was investigated as described in Supplementary data^{76–78}.

4.3. Docking studies

Molecular docking studies of the synthesised compounds were carried out against EGFR^{WT} (PDB ID: 4HJO, resolution 2.75 Å) and EGFR^{T790M} (PDB ID: 3W2O, resolution 2.35 Å) as described in Supplementary data²².

Acknowledgement

This paper is based upon work supported by Science, Technology & Innovation Funding Authority (STIFA) under grant number 43327.

Disclosure statement

No potential conflict of interest was reported by the author(s).

Funding

This paper is based upon work supported by Science, Technology & Innovation Funding Authority (STIFA) under [grant number 43327].

ORCID

Heba S. A. Elzahabi  <http://orcid.org/0000-0002-7023-6364>

Ibrahim H. Eissa  <http://orcid.org/0000-0002-6955-2263>

References

- WHO. Cancer. Available from: <https://www.who.int/news-room/fact-sheets/detail/cancer>. (last accessed 13 Jan 2022).
- Boyle P, Ferlay JJ. Cancer incidence and mortality in Europe, 2004. *Annals Oncol* 2005;16:481–8.
- Gavalas NG, Karadimou A, Dimopoulos MA, et al. Immune response in ovarian cancer: how is the immune system involved in prognosis and therapy: potential for treatment utilization. *J Immunol Res* 2010;2010:1–15.
- Li M, Huo X, Davuljigari CB, et al. MicroRNAs and their role in environmental chemical carcinogenesis. *Environ Geochem Health* 2019;41:225–47.
- Chorawala M, Oza P, Shah GJ. Mechanisms of anticancer drugs resistance: an overview. *J Pharm Technol Drug Res* 2012;4:1–9.
- Lavogina D, Enkvist E, Uri A. Bisubstrate inhibitors of protein kinases: from principle to practical applications. *ChemMedChem* 2010;5:23–34.
- Luković E, González-Vera JA, Imperiali B. Recognition-domain focused chemosensors: versatile and efficient reporters of protein kinase activity. *J Am Soc* 2008;130:12821–7.
- Braun T, Gautel MJ. Transcriptional mechanisms regulating skeletal muscle differentiation, growth and homeostasis. *Nat Rev Mol cell Biol* 2011;12:349–61.
- Meulenbeld HJ, Mathijssen RH, Verweij J, et al. Danusertib, an aurora kinase inhibitor. *Expert Opin Investig Drugs* 2012; 21:383–93.
- Abdellatif KR, Bakr RB. Pyrimidine and fused pyrimidine derivatives as promising protein kinase inhibitors for cancer treatment. *Med Chem J* 2021;30:31–49.
- Ullrich A, Schlessinger J. Signal transduction by receptors with tyrosine kinase activity. *Cell* 1990;61:203–12.
- Voldborg BR, Damstrup L, Spang-Thomsen M, Poulsen HS. Epidermal growth factor receptor (EGFR) and EGFR mutations, function and possible role in clinical trials. *Ann Oncol* 1997;8:1197–206.
- Meierjohann S, Mueller T, Scharl M, Buehner MJ. A structural model of the extracellular domain of the oncogenic EGFR variant Xmrk. *Zebrafish* 2006;3:359–69.
- Ren S, Chen X, Kuang P, et al. Association of EGFR mutation or ALK rearrangement with expression of DNA repair and synthesis genes in never-smoker women with pulmonary adenocarcinoma. *Cancer* 2012;118:5588–94.
- Normanno N, De Luca A, Bianco C, et al. Epidermal growth factor receptor (EGFR) signaling in cancer. *Gene* 2006;366: 2–16.
- Godin-Heymann N, Ulkus L, Brannigan BW, et al. The T790M “gatekeeper” mutation in EGFR mediates resistance to low concentrations of an irreversible EGFR inhibitor. *Mol Cancer Ther* 2008;7:874–9.
- Abdelsalam EA, Zaghary WA, Amin KM, et al. Synthesis and in vitro anticancer evaluation of some fused indazoles, quinazolines and quinolines as potential EGFR inhibitors. *Bioorg Chem* 2019;89:102985.
- Ismail RS, Abou-Seri SM, Eldehna WM, et al. Novel series of 6-(2-substitutedacetamido)-4-anilinoquinazolines as EGFR-ERK signal transduction inhibitors in MCF-7 breast cancer cells. *Eur J Med Chem* 2018;155:782–96.
- Gandin V, Ferrarese A, Dalla Via M, et al. Targeting kinases with anilino-pyrimidines: discovery of N-phenyl-N'-[4-(pyrimidin-4-ylamino)phenyl]urea derivatives as selective inhibitors of class III receptor tyrosine kinase subfamily. *Sci Rep* 2015; 5:16750.
- Traxler P, Furet P. Strategies toward the design of novel and selective protein tyrosine kinase inhibitors. *Pharmacol Therapeutics* 1999;82:195–206.
- Zhang J, Yang PL, Gray NS. Targeting cancer with small molecule kinase inhibitors. *Nat Rev Cancer* 2009;9:28–39.
- Gaber AA, Bayoumi AH, El-Morsy AM, et al. Design, synthesis and anticancer evaluation of 1H-pyrazolo[3,4-d]pyrimidine derivatives as potent EGFRWT and EGFR T790M inhibitors and apoptosis inducers. *Bioorg Chem* 2018;80:375–95.
- Sharma VK, Nandekar PP, Sangamwar A, et al. Structure guided design and binding analysis of EGFR inhibiting analogues of erlotinib and AEE788 using ensemble docking, molecular dynamics and MM-GBSA. *RSC Adv* 2016;6: 65725–35.
- Mowafy S, Galanis A, Doctor ZM, et al. Toward discovery of mutant EGFR inhibitors; design, synthesis and in vitro biological evaluation of potent 4-aryl-amino-6-ureido and thiourido-quinazoline derivatives. *Biorg Med Chem* 2016;24: 3501–12.
- Zhao Z, Wu H, Wang L, et al. Exploration of type II binding mode: a privileged approach for kinase inhibitor focused drug discovery? *ACS Chem Biol* 2014;9:1230–41.
- Liu Y, Gray NS. Rational design of inhibitors that bind to inactive kinase conformations. *Nat Chem Biol* 2006;2:358–64.
- Bonomi P. Erlotinib: a new therapeutic approach for non-small cell lung cancer. *Expert Opin Invest Drugs* 2003;12: 1395–401.
- Pao W, Wang TY, Riely GJ, et al. KRAS mutations and primary resistance of lung adenocarcinomas to gefitinib or erlotinib. *PLoS Med* 2005;2:e17.
- Pao W, Miller VA, Politi KA, et al. Acquired resistance of lung adenocarcinomas to gefitinib or erlotinib is associated with a second mutation in the EGFR kinase domain. *PLOS Med* 2005;2:e73.
- Kobayashi S, Boggon TJ, Dayaram T, et al. EGFR mutation and resistance of non-small-cell lung cancer to gefitinib. *N Engl J Med* 2005;352:786–92.
- Kwak EL, Sordella R, Bell DW, et al. Irreversible inhibitors of the EGF receptor may circumvent acquired resistance to gefitinib. *Proc Natl Acad Sci USA* 2005;102:7665–70.
- Engelman JA, Zejnullahu K, Gale C-M, et al. PF00299804, an irreversible pan-ERBB inhibitor, is effective in lung cancer models with EGFR and ERBB2 mutations that are resistant to gefitinib. *Cancer Res* 2007;67:11924–32.

33. Li D, Ambrogio L, Shimamura T, et al. BIBW2992, an irreversible EGFR/HER2 inhibitor highly effective in preclinical lung cancer models. *Oncogene* 2008;27:4702–11.
34. Sohn SH, Sul HJ, Kim B, et al. RNF43 and PWWP2B inhibit cancer cell proliferation and are predictive or prognostic biomarker for FDA-approved drugs in patients with advanced gastric cancer. *J Cancer*. 2021;12:4616–25.
35. Sequist LV, Besse B, Lynch TJ, et al. Neratinib, an irreversible pan-ErbB receptor tyrosine kinase inhibitor: results of a phase II trial in patients with advanced non-small-cell lung cancer. *J Clin Oncol* 2010;28:3076–83.
36. Kim Y, Ko J, Cui Z, et al. The EGFR T790M mutation in acquired resistance to an irreversible second-generation EGFR inhibitor. *Mol Cancer Therapeutics* 2012;11:784–91.
37. Jänne PA, Yang JC-H, Kim D-W, et al. AZD9291 in EGFR inhibitor-resistant non-small-cell lung cancer. *N Engl J Med* 2015;372:1689–99.
38. J. Carroll. Following lethal tox report, Boehringer scraps plans for high-speed development, kills \$730M Hanmi deal; 2016. Available from: <https://endpts.com/following-lethal-tox-report-boehringer-scrap-plans-for-high-speed-development-kills-730m-hanmi-deal/>. (last accessed May 2019).
39. P, Callery G, Peter Cancer and cancer chemotherapy. In: David, AW and Thomas, LL, eds. Foye's principles of medical chemistry. Philadelphia: Lippincott, Williams and Wilkins; 2002.
40. Abdel-Mohsen HT, Ragab FA, Ramla MM, El Diwani HI. Novel benzimidazole-pyrimidine conjugates as potent antitumor agents. *Eur J Med Chem* 2010;45:2336–44.
41. Shao H, Shi S, Foley DW, et al. Synthesis, structure-activity relationship and biological evaluation of 2,4,5-trisubstituted pyrimidine CDK inhibitors as potential anti-tumour agents. *Eur J Med Chem* 2013;70:447–55.
42. Fathalla O, Zeid I, Haiba M, et al. Synthesis, antibacterial and anticancer evaluation of some pyrimidine derivatives. *World J Chem* 2009;4:127–32.
43. Yu L, Huang M, Xu T, et al. A structure-guided optimization of pyrido[2,3-d]pyrimidin-7-ones as selective inhibitors of EGFR L858R/T790M mutant with improved pharmacokinetic properties. *Eur J Med Chem* 2017;126:1107–17.
44. Xu T, Peng T, Ren X, et al. C5-substituted pyrido [2, 3-d] pyrimidin-7-ones as highly specific kinase inhibitors targeting the clinical resistance-related EGFR T790M mutant. *MedChemComm* 2015;6:1693–7.
45. El-Naggar AM, Abou-El-Regal MM, El-Metwally SA, et al. Synthesis, characterization and molecular docking studies of thiouracil derivatives as potent thymidylate synthase inhibitors and potential anticancer agents. *Mol Div* 2017;21:967–83.
46. Eldehna WM, Abo-Ashour MF, Nocentini A, et al. Novel 4/3-((4-oxo-5-(2-oxoindolin-3-ylidene)thiazolidin-2-ylidene)amino) benzenesulfonamides: synthesis, carbonic anhydrase inhibitory activity, anticancer activity and molecular modelling studies. *Eur J Med Chem* 2017;139:250–62.
47. El-Naggar AM, Eissa IH, Belal A, El-Sayed AA. Design, eco-friendly synthesis, molecular modeling and anticancer evaluation of thiazol-5 (4H)-ones as potential tubulin polymerization inhibitors targeting the colchicine binding site. *RSC Adv* 2020;10:2791–811.
48. Eissa IH, El-Naggar AM, El-Hashash MA. Design, synthesis, molecular modeling and biological evaluation of novel 1H-pyrazolo[3,4-b]pyridine derivatives as potential anticancer agents. *Bioorg Chem* 2016;67:43–56.
49. Eissa IH, El-Naggar AM, Abd El-Sattar NE, Youssef AS. Design and discovery of novel quinoxaline derivatives as dual DNA intercalators and topoisomerase II inhibitors. *Anti-Cancer Agents Med Chem* 2018;18:195–209.
50. Ibrahim M, Taghour M, Metwaly A, et al. Design, synthesis, molecular modeling and anti-proliferative evaluation of novel quinoxaline derivatives as potential DNA intercalators and topoisomerase II inhibitors. *Eur J Med Chem* 2018;155:117–34.
51. Eissa IH, Metwaly AM, Belal A, et al. Discovery and antiproliferative evaluation of new quinoxalines as potential DNA intercalators and topoisomerase II inhibitors. *Archiv der Pharmazie* 2019;352:1900123.
52. Mahdy HA, Ibrahim MK, Metwaly AM, et al. Design, synthesis, molecular modeling, in vivo studies and anticancer evaluation of quinazolin-4(3H)-one derivatives as potential VEGFR-2 inhibitors and apoptosis inducers. *Bioorg Chem* 2020;94:103422.
53. El-Helby AGA, Sakr H, Eissa IH, et al. Benzoxazole/benzothiazole-derived VEGFR-2 inhibitors: design, synthesis, molecular docking, and anticancer evaluations. *Archiv der Pharmazie* 2019;352:1900178.
54. Elmetwally SA, Saied KF, Eissa IH, Elkaeed EB. Design, synthesis and anticancer evaluation of thieno[2,3-d]pyrimidine derivatives as dual EGFR/HER2 inhibitors and apoptosis inducers. *Bioorg Chem* 2019;88:102944.
55. Nasser AA, Eissa IH, Oun MR, et al. Discovery of new pyrimidine-5-carbonitrile derivatives as anticancer agents targeting EGFRWT and EGFR T790M. *Org Biomol Chem* 2020;18:7608–34.
56. Othman IM, Alamshany ZM, Tashkandi NY, et al. New pyrimidine and pyrazole-based compounds as potential EGFR inhibitors: synthesis, anticancer, antimicrobial evaluation and computational studies. *Bioorg Chem* 2021;114:105078.
57. Abd El-Meguid EA, Moustafa GO, Awad HM, et al. Novel benzothiazole hybrids targeting EGFR: design, synthesis, biological evaluation and molecular docking studies. *Anticancer Agents Med Chem* 2021;1240:130595.
58. Khattab RR, Alshamari AK, Hassan AA, et al. Click chemistry based synthesis, cytotoxic activity and molecular docking of novel triazole-thienopyrimidine hybrid glycosides targeting EGFR. *J Enzyme Inhib Med Chem* 2021;36:504–16.
59. Elzahabi HS, Nossier ES, Khalifa NM, et al. Anticancer evaluation and molecular modeling of multi-targeted kinase inhibitors based pyrido[2,3-d]pyrimidine scaffold. *J Enzyme Inhib Med Chem* 2018;33:546–57.
60. Khalifa NM, Adel A-H, Abd-Elmoez SI, et al. A convenient synthesis of some new fused pyridine and pyrimidine derivatives of antimicrobial profiles. *Res Chem Intermed* 2015;41:2295–305.
61. Mosmann T. Rapid colorimetric assay for cellular growth and survival: application to proliferation and cytotoxicity assays. *J Immunol Methods* 1983;65:55–63.
62. Denizot F, Lang RJoim. Rapid colorimetric assay for cell growth and survival: modifications to the tetrazolium dye procedure giving improved sensitivity and reliability. *J Immunol Methods* 1986;89:271–7.
63. Thabrew MI, Hughes RD, McFarlane IGJ. Screening of hepatoprotective plant components using a HepG2 cell cytotoxicity assay. *J Pharm Pharmacol* 2011;49:1132–5.
64. Jia Y, Quinn CM, Gagnon AI, Talanian R. Homogeneous time-resolved fluorescence and its applications for kinase assays in drug discovery. *Anal Biochem* 2006;356:273–81.

65. Wang J, Lenardo MJ. Roles of caspases in apoptosis, development, and cytokine maturation revealed by homozygous gene deficiencies. *J Cell Sci* 2000;113:753–7.
66. Vermes I, Haanen C, Steffens-Nakken H, Reutelingsperger C. A novel assay for apoptosis flow cytometric detection of phosphatidylserine expression on early apoptotic cells using fluorescein labelled annexin V. *J Immunol Methods* 1995; 184:39–51.
67. Earnshaw WC, Martins LM, Kaufmann SH. Mammalian caspases: structure, activation, substrates, and functions during apoptosis. *Ann Rev Biochem* 1999;68:383–424.
68. Bortner CD, Cidlowski JA. Apoptotic volume decrease and the incredible shrinking cell. *Cell Death Different* 2002;9: 1307–10.
69. Bae SS, Choi JH, Oh YS, et al. Proteolytic cleavage of epidermal growth factor receptor by caspases. *FEBS Lett* 2001;491: 16–20.
70. He Y, Huang J, Chignell C. Cleavage of epidermal growth factor receptor by caspase during apoptosis is independent of its internalization. *Oncogene* 2006;25:1521–31.
71. Park JH, Liu Y, Lemmon MA, Radhakrishnan R. Erlotinib binds both inactive and active conformations of the EGFR tyrosine kinase domain. *Biochem J* 2012;448:417–23.
72. Sogabe S, Kawakita Y, Igaki S, et al. Structure-based approach for the discovery of pyrrolo[3,2-d]pyrimidine-based EGFR T790M/L858R mutant inhibitors. *ACS Med Chem Lett* 2013;4:201–5.
73. Taylor EC, Cheng C. Studies in purine chemistry. VI. A convenient one-step synthesis of hypoxanthine. *J Am Chem Soc* 1959;1:9–11.
74. Eldehna WM, Hassan GS, Al-Rashood ST, et al. Synthesis and in vitro anticancer activity of certain novel 1-(2-methyl-6-arylpyridin-3-yl)-3-phenylureas as apoptosis-inducing agents. *J Enzyme Inhib Med Chem* 2019;34:322–32.
75. Al-Warhi T, Abo-Ashour MF, Almahli H, et al. Novel [(N-alkyl-3-indolylmethylene)hydrazono]oxindoles arrest cell cycle and induce cell apoptosis by inhibiting CDK2 and Bcl-2: synthesis, biological evaluation and in silico studies. *J Enzyme Inhib Med Chem* 2020;35:1300–9.
76. Lo KK-W, Lee TK-M, Lau JS-Y, et al. Luminescent biological probes derived from ruthenium(II) estradiol polypyridine complexes. *Inorg Chem* 2008;47:200–8.
77. Sabt A, Abdelhafez OM, El-Haggar RS, et al. Novel coumarin-6-sulfonamides as apoptotic anti-proliferative agents: synthesis, in vitro biological evaluation, and QSAR studies. *J Enzyme Inhib Med Chem* 2018;33:1095–107.
78. Al-Sanea MM, Al-Ansary GH, Elsayed ZM, et al. Development of 3-methyl/3-(morpholinomethyl)benzofuran derivatives as novel antitumor agents towards non-small cell lung cancer cells. *J Enzyme Inhib Med Chem* 2021;36:987–99.